Author for correspondence:
Maryam Sheibi, Email: sheibi@sharoodut.ac.ir

CAMBRIDGE
UNIVERSITY PRESS

Ballooning emplacement and alteration of the Chah-Musa subvolcanic intrusion (NE Iran) inferred from magnetic susceptibility and fabric

Ali Seifivand and Maryam Sheibi [ORCID]

Faculty of Earth Sciences, Shahrood University of Technology, Shahrood, Iran

Abstract

The porphyritic diorite Chah-Musa subvolcanic intrusion is located in the Toroud-Chah Shirin magmatic arc in the northern Central Iranian structural zone. The elliptical Chah-Musa body hosts a copper deposit and intrudes an Eocene sequence of volcanic breccia, agglomerate and red tuffaceous sediment. High magnetic susceptibility values are attributed to the presence of magnetite as a magnetic carrier. Changes in bulk magnetic susceptibility correlate with zonation of alteration in the intrusion. Although the degree of anisotropy of magnetic susceptibility decreases due to hydrothermal alteration, the field observations confirm that this parameter can be used as a strain marker. Strongly oblate magnetic ellipsoids are found in the eastern half of the intrusion where isolated outcrops of flat-lying tuffaceous host cover dioritic rocks (roof zone). Stations with prolate ellipsoids mostly belong to the centre of the intrusion where the magnetic lineations plunge steeply. They are interpreted as indicating the main feeder zone. The concentric fabric pattern at the periphery of intrusion, the oblate magnetic ellipsoids at the roof, the highest anisotropy degree along the small diameter of the intrusion, and an intense deformation of the host rocks, especially at the western margin, all are evidence that the intrusion was ballooning during the late stages of its emplacement. Ascent and emplacement of the Chah-Musa body is ascribed to the tensional space provided by a dextral shear zone created by the regional left-lateral movement on the bounding Anjilow and Toroud strike-slip faults.

1. Introduction

The Toroud – Chah Shirin (TCS) magmatic arc (Fig. 1a) is one of several mineralized belts in the structural zone of central Iran (Houshmandzadeh *et al.* 1978). Magmatic activity in this region relates to the Tertiary northward subduction of the Sabzevar–Darouneh branch of the Neo-Tethys ocean (Yousefi *et al.* 2017). The TCS magmatic arc comprises a 100 km × 10 km uplifted block bounded by the Toroud fault to the south, and the Anjilow fault to the north (Fig. 1b). In this block, NE–SW-trending volcano-intrusive rocks consist mainly of middle- to upper-Eocene andesites and dacites, and Oligocene diorites. Middle Eocene tuff, shale, marl and sandstone are associated with the igneous rocks (Houshmandzadeh *et al.* 1978; Fodazi & Emami, 2000). Although these geologic relationships are clearly related to subduction (e.g. A Jafarian, unpub. MSc thesis, Univ. Tehran, 1988; Rashidnejad-Omran, 1992; Imamjome *et al.* 2009; Khajehzadeh, 2012; Khalaj, 2016), the tectono-magmatic processes of magma emplacement in the TCS magmatic arc have not been studied. We shall investigate this aspect along with the changes in magnetic fabric caused by the hydrothermal alteration that accompanied copper mineralization.

Shallow emplacement of magma is associated with formation of mineral deposits (e.g. porphyry-copper type), geothermal fields, maturation of hydrocarbon reservoirs in sedimentary basins (e.g. Jones *et al.* 2007), and even global climate change (Svensen *et al.* 2008). The TCS magmatic arc hosts many epithermal ore deposits (Rashidnejad-Omran, 1992; Sengör *et al.* 1993; Tajeddin, 1999; Shamanian *et al.* 2004; Fard *et al.* 2006; Imamjome *et al.* 2009; Mehrabi & Ghasemi, 2012; Mehrabi *et al.* 2015). In this paper we report a detailed petrogenetic investigation of the Chah-Musa district undertaken as a strategy for effective exploration. Geologic information about the Chah-Musa Cu deposit is scarce in spite of its importance. This paper describes the mechanism of emplacement of the Chah-Musa body, a subvolcanic intrusion located in the northern part of the TCS magmatic arc (Fig. 1). This calc-alkaline intrusion (35° 29′ N, 54° 52′ E), which hosts a high copper anomaly, has been previously investigated by several authors (Imamjome *et al.* 2009; Khajehzadeh, 2012; Khalaj, 2016). Since fabric measurements in the field are difficult, the anisotropy of magnetic susceptibility (AMS) technique is here used as a proxy to reveal magma flow directions, feeder zones and mode of final emplacement.
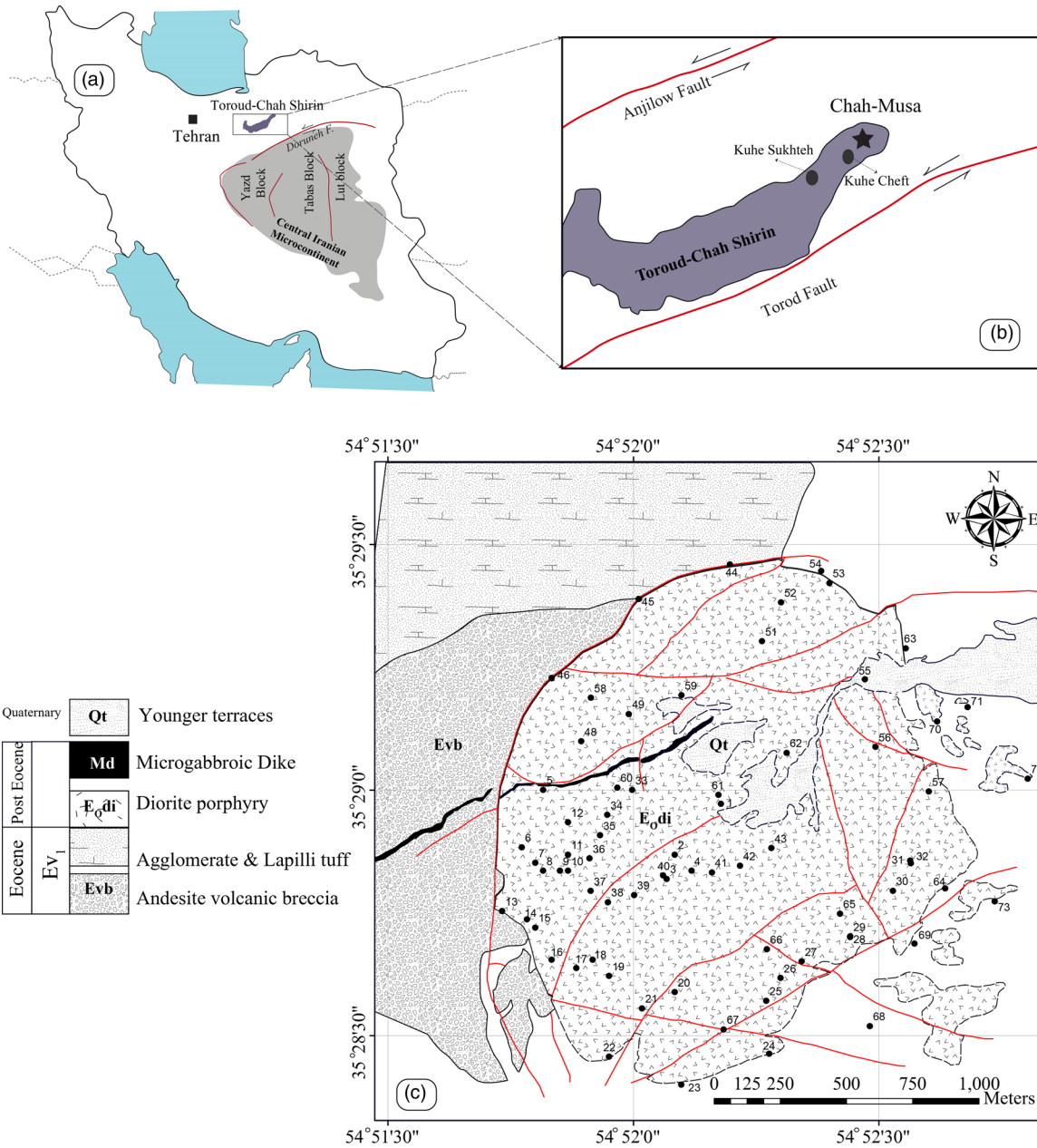
Fig. 1. (Colour online) (a) Location of Toroud – Chah Shirin (TCS) magmatic arc in Iran. (b) Schematic structural map of the TCS arc which is bounded by sinistral NE-striking Anjilow and Toroud regional faults (Houshmandzadeh *et al.* 1978). A star denotes the study area. (c) Simplified geological map of Chah-Musa pluton. Labelled black dots show locations where 73 samples were drilled for AMS study.

2. Regional geology

The TCS magmatic arc which trends N60–70°E, consists mainly of Palaeogene igneous rocks, although including scattered outcrops of metamorphosed Palaeozoic and Mesozoic rocks. Middle to possibly late Eocene igneous activity (Houshmandzadeh *et al.* 1978) consists of: (1) explosively deposited rhyolitic to rhyodacitic tuffs and local andesitic lava flows, associated with marls, tuffaceous marlstones and sandstones; (2) lava flows and pyroclastic rocks of andesite, trachy-andesite and basaltic andesite; and (3) subordinate dacitic–rhyodacitic rocks and hypabyssal intrusive rocks. The TCS magmatic arc is bounded by the Toroud and Anjilow faults that have the same trends, nearly vertical dip and sinistral movements (Houshmandzadeh *et al.* 1978). Mehrabi *et al.* (2015)

analysedthe spatial distribution of 12 epithermal deposits using Fry (1979) and point pattern analysis in order to infer geologic controls. Their data are consistent with a Riedel shear model in which sinistral NE-striking faults and lineaments (i.e. the Anjilow and Toroud faults) represent the main shear plane, and the NNW and WNW structures represent R and R′, respectively (Fig. 2).

The oldest exposed rocks include Eocene volcanic breccia (*c.* 400 m thick in the west) and red tuffaceous and agglomerate assemblages that crop out especially adjacent to the northern and northwestern parts of the Chah-Musa subvolcanic intrusion (Fig. 3a, c). Eocene tuffaceous rocks (E_t) occur along the northern border (Fig. 3a, b). The tuff is dark red to purple thin-laminated (Fig. 3b), containing lithics and interlayers of dacitic lava (E_{dc}).
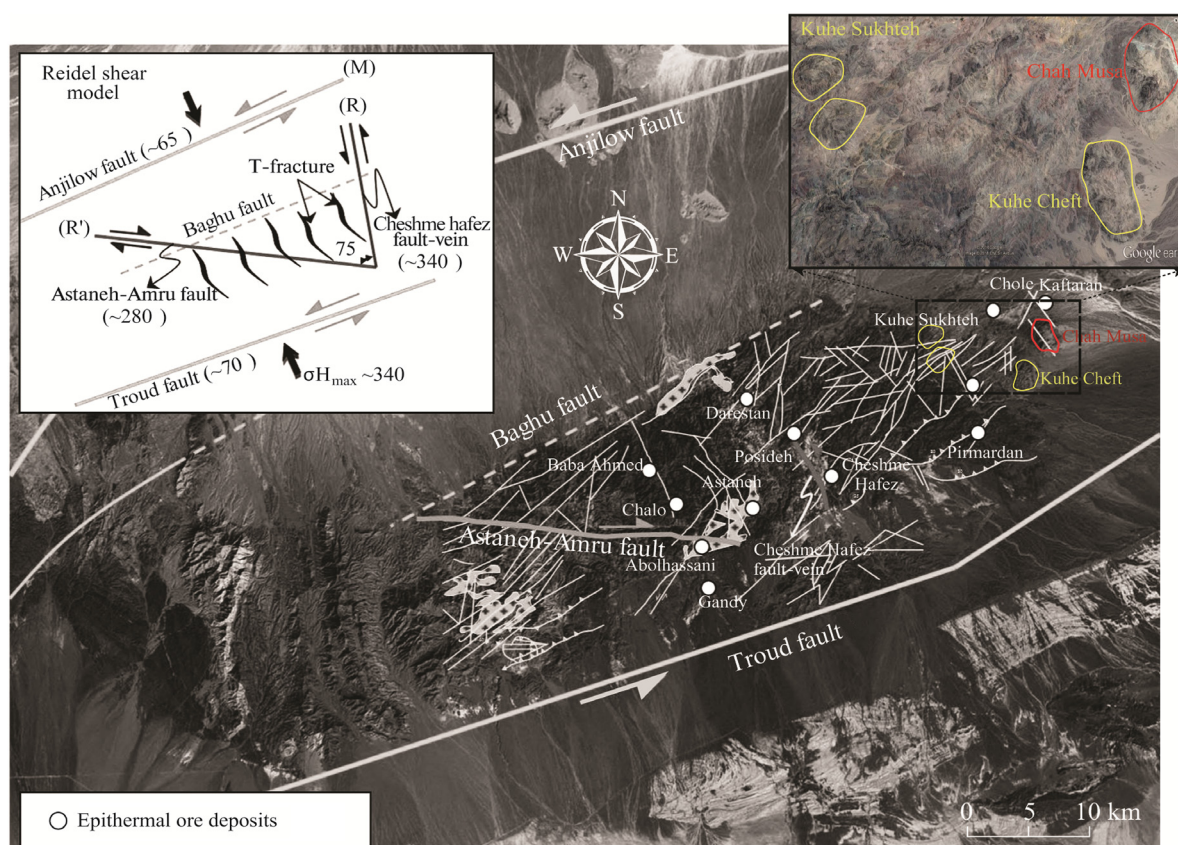
Fig. 2. (Colour online) Landsat image showing the structural model and location of epithermal ore deposit in the TCS belt. The model includes the NE-striking regional sinistral faults (F1, ~70°), sinistral NNW-striking faults (F2, ~340°) and dextral WNW-striking faults (F3, ~280°). The orientation of σH-max, modelled as the acute bisector of the conjugate pair, is ~340° and the majority of veins are modelled as nearly pure extension fractures (T) oriented roughly parallel to σH-max. The model fits well with the Riedel shear model in which sinistral NE-striking faults and lineaments represent the main shear plane (M), and the NNW structures and WNW structures represent R and R′, respectively (Mehrabi *et al.* 2015).

Large isolated outcrops of this flat-lying host rock exist in the eastern margins of the intrusion. Its western margin is surrounded by pyroclastic rocks including andesitic agglomerates (E_{ag}), and volcanic breccias (E_{vb}) contain angular fragments up to 50 cm in size (Fig. 3e). Agglomerates mostly consist of lava fragments of various sizes and shapes. The occurrence of small to large fragments of red tuff (Fig. 3d) in this unit confirms that the agglomerates and breccias are located at the top of the Eocene volcanoclastic sequence.

The Chah-Musa porphyritic hornblende diorite intrusion, emplaced into the Eocene volcanic sequence, is enclosed in a narrow, low-grade contact metamorphic halo consistent with shallow-level emplacement. The intrusion is roughly elliptical (1.5 × 2.3 km; Figs 1c, 4a). Hand specimens exhibit a porphyritic structure with *c.* 40% phenocrysts (Fig. 4b). Two kinds of contact can be distinguished: (1) a primary, undeformed emplacement contact, moderately dipping to the west, parallel to bedding of the host rocks in the NE part of the intrusion (Fig. 3a); and (2) a western contact associated with extremely crushed host rocks (Fig. 3c) along the inner contact of the intrusion. The latter contact is manifested as onion-skin erosion of the porphyritic diorite (Fig. 4c) that is attributed not to weathering processes but rather, to pressure release expansion due to erosion of the overlying rocks, and creation of curved joints under conditions of radial compressive stress. A mafic dyke of microgabbro, more than 1.8 km in length, 4–10 m in thickness and NE–SW in trend, intrudes the Chah-Musa

intrusion and its volcanic host. To the east, the contact is covered by Quaternary alluvium.

The summit of the Chah-Musa body is at the centre of the intrusion, close to station #40 (Figs 1c, 4a). According to field studies, plagioclase phenocrysts, dark hornblende needles and platy biotites occur in the least altered eastern peripheral part of the intrusion. In the central part of the intrusion, of light creamy colour, large plagioclase phenocrysts and opacified hornblende ± biotite are present, consistent with sericite/quartz (phyllitic) alteration (right side of Fig. 4a). Weak chlorite/calcite (propylitic) alteration appears in the outer margin of the intrusion. Intense propylitic alteration (replacement by epidote, chlorite, calcite and pyrite) is observed in boreholes at depths of 70 to 90 m. The soft, light-brown to yellow argillic zone commonly contains hematite, limonite and clay minerals. Propylitic and phyllitic alterations are overprinted by argillic alteration, especially along the main fractures. Supergene processes are responsible for the formation of extensive alteration of hypogene sulphide minerals such as bornite, pyrite, minor chalcopyrite to secondary chalcocite, covellite, digenite, malachite and neotocite (Imamjome *et al.* 2009).

Elongate xenoliths of different sizes are abundant at the borders of the intrusion (Fig. 4d). Their preferred orientations at the western margin of the intrusion suggest that an increasing strain had been imposed during intrusion. Toward the centre of the intrusion, small xenoliths appear to be randomly distributed (Fig. 4e).
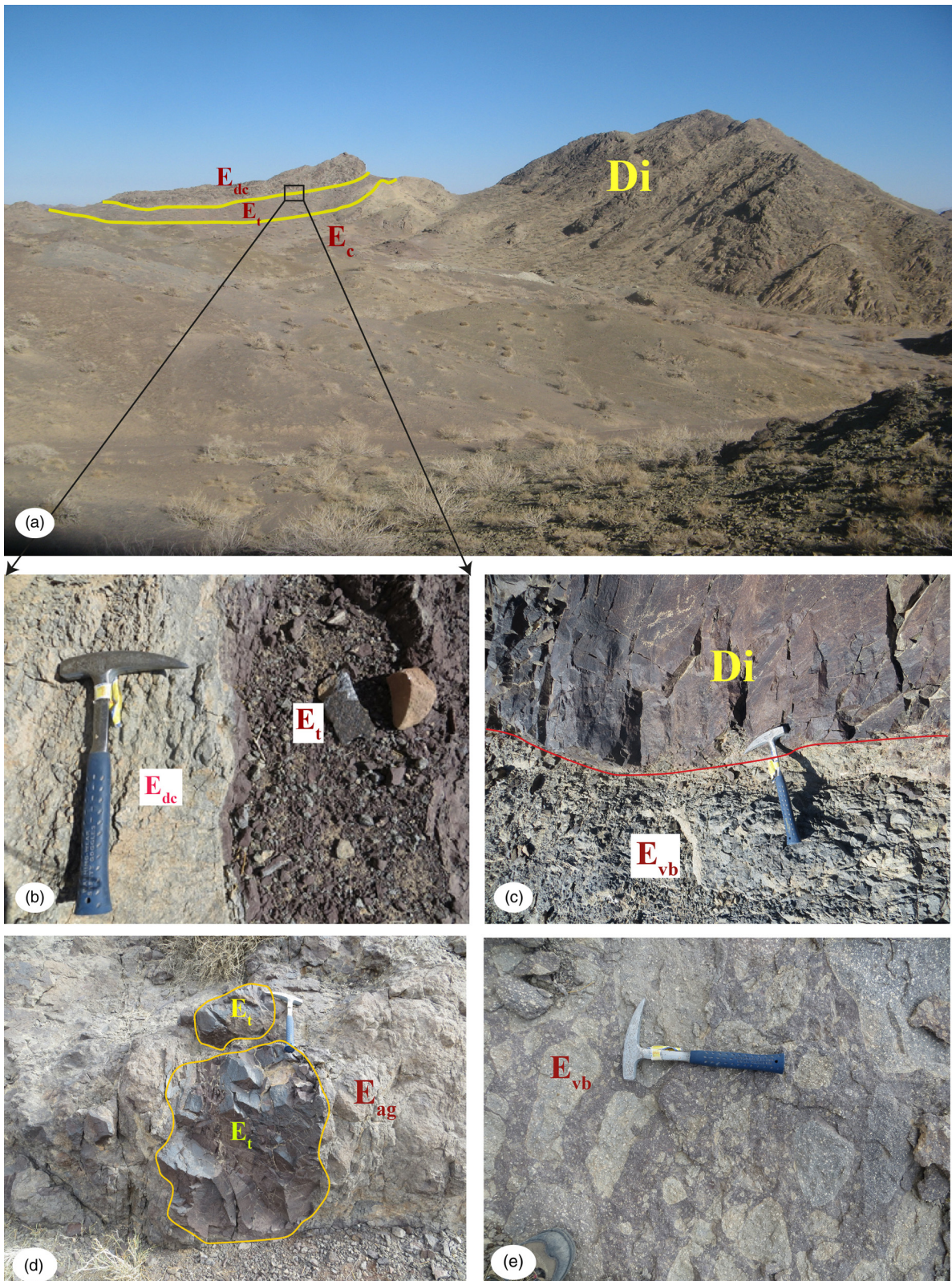
Fig. 3. (Colour online) Field views of the Eocene volcano-pyroclastic sequence (Ev_1) that is the main host rock of the Chah-Musa intrusion. (a) Northwestern contact of the Chah-Musa sub-volcanic intrusion parallel to bedding in the country rocks where red tuff and dacitic lava are inclined. (b) Sharp contact between Eocene dacitic lava (E_{dc}) and red tuff (E_t). (c) Closer view of the contact of diorite porphyry (Di) with extremely crushed host rocks (Ev_b) along the western border. (d) Typical agglomerate (E_{ag}) containing large fragments of red tuff (E_t). (e) Volcanic breccia at the top of the host sequence.

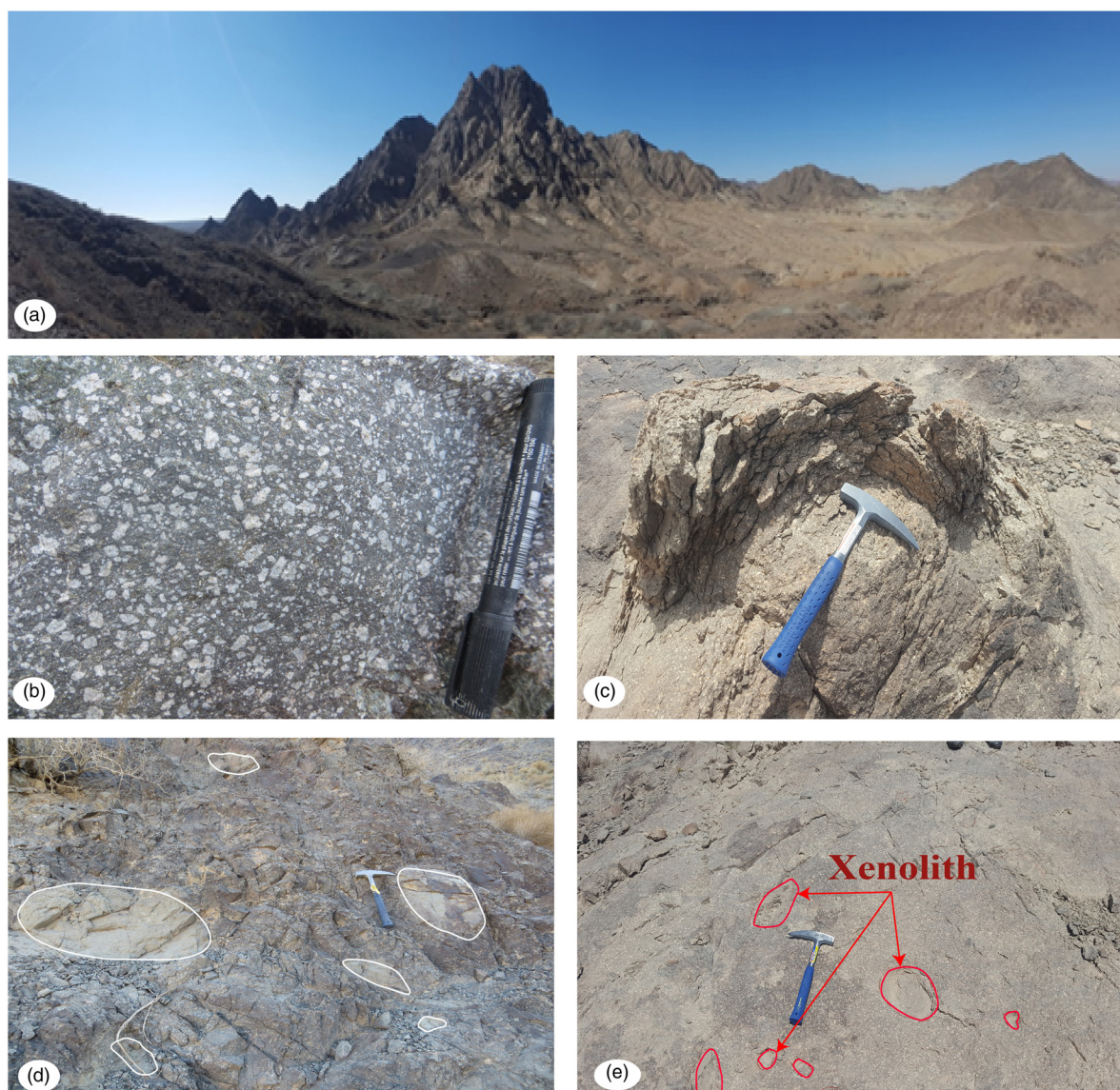**Fig. 4.** (Colour online) (a) Field view of the Chah-Musa intrusion. Landscape of the summit and low-elevation flat area of Chah-Musa. (b) Hand specimen of fresh porphyritic diorite containing phenocrysts of plagioclase and needles of hornblende set in a fine-grained matrix. (c) Onion skin erosion of the porphyry diorite at the western inner contact. (d) and (e) respectively show some xenoliths with preferred orientation parallel to the innermost margin, and small randomly disseminated xenoliths at the centre of the intrusion.

3. Field and laboratory techniques

Fieldwork was aimed at collecting structural data and a representative suite of samples. A minimum of two 25 mm diameter oriented core cylinders were collected at each station. In all, 73 stations provided 674 core samples, 2.2 cm in height (Fig. 1c). After preparation of the latter, the magnetic fabric (AMS) was measured with a Kappabridge MFK1-FA susceptometer (AGICO) at the Geomagnetic Laboratory, Shahrood University of Technology, Iran. The instrument operates at low field frequency (4×10^{-4} T; 920 Hz). Orientations and magnitudes of the three principal axes of the AMS ellipsoids ($K_1 \geq K_2 \geq K_3$) were obtained for each sampling station, through the tensor average of the individual AMS measurements. Bulk susceptibility (Km) is the mean value of the magnitudes of the three axes of the AMS ellipsoid: $Km = 1/3(K_1 + K_2 + K_3)$. The anisotropy percentage P% = $100[(K_1/K_3) – 1]$ and the shape parameter $T = \ln[K_2/(K_1/K_3)]/\ln[K_1/K_3]$ (Jelinek, 1978) were calculated for each sampling station.

A positive shape parameter (T < 0) corresponds to an oblate ellipsoid, a negative parameter (T > 0) to a prolate ellipsoid. The magnetic foliation plane contains the K_1 and K_2 axes, and the magnetic lineation is parallel to K_1 in this plane. The values of scalar parameters (Km, P%, T) and the orientation data (foliation and lineation) for each station are given in Table 1.

In addition, we prepared 73 thin-sections for petrographic and microstructural study. Identification of the basic magnetic mineralogy responsible for the susceptibility and its anisotropy was performed using a CS-2 furnace (AGICO) coupled to a KLY-2 susceptometer located in the Palaeomagnetic Laboratory of the Geological Survey of Iran, Tehran. This device records the susceptibility variation (Km) as a function of temperature from 20 °C to 700 °C. Analysis of the regional tectonics, the AMS measurements and petrographic observations of thin-sections comprise the database for interpretation of the emplacement mechanism of the Chah-Musa intrusion.

Table 1. Anisotropy of magnetic susceptibility data of the Chah-Musa intrusion

Station	N	Long.	Lat.	Km	P%	T	K1.Trend	K1.Plunge	K3.Strike	K3.Dip
1	6	54.8696	35.4829	4.64	2.7	−0.5	150	17	352	40
2	9	54.8681	35.4811	3.63	5	−0.6	28	65	339	70
3	5	54.8678	35.4803	5.18	6.6	−0.4	334	70	106	14
4	6	54.8686	35.4806	9.94	3.3	−0.2	19	27	248	35
5	8	54.8636	35.4833	3.83	5.5	−0.2	137	16	99	25
6	6	54.8629	35.4814	9.51	2.9	−0.2	183	3	10	22
7	7	54.8633	35.4808	5.54	2.6	−0.1	12	40	300	41
8	6	54.8636	35.4806	3.03	4	0.5	335	66	259	66
9	7	54.8642	35.4806	0.415	1.3	0.1	105	14	100	69
10	11	54.8644	35.4806	1.15	1.4	−0.3	79	6	64	23
11	10	54.8644	35.4811	10.1	2.4	0.1	11	1	196	10
12	8	54.8644	35.4822	5.46	5.1	0.1	60	63	260	80
13	7	54.8622	35.4792	1.4	1.7	0	345	19	202	30
14	7	54.8631	35.4789	0.479	1.6	−0.2	139	16	354	27
15	9	54.8633	35.4786	0.925	2.8	0	53	39	27	61
16	10	54.8639	35.4775	0.462	1.1	−0.1	71	10	253	82
17	9	54.8647	35.4772	3.83	4.2	−0.3	90	63	281	85
18	7	54.8653	35.4775	12.8	5.5	0.4	64	45	287	56
19	8	54.8658	35.4769	10.8	7.6	−0.3	202	41	105	41
20	10	54.8681	35.4764	0.979	1.1	−0.5	128	40	9	43
21	9	54.8669	35.4758	1.76	1.8	−0.1	212	13	53	32
22	9	54.8658	35.4742	1.07	1.2	0.3	76	25	34	35
23	11	54.8684	35.4728	12.4	5.5	0.6	98	53	68	69
24	9	54.8713	35.4741	15.7	6.3	−0.7	230	40	193	54
25	8	54.8711	35.4761	11.3	7.7	0.3	165	22	346	87
26	8	54.8716	35.4769	8.7	6.5	−0.7	326	10	147	85
27	7	54.8723	35.4774	11.8	7.3	0.5	206	15	204	80
28	12	54.874	35.4783	8.64	7.9	0.3	182	30	2	90
29	8	54.874	35.4783	7.97	7.1	−0.1	66	18	257	61
30	10	54.8754	35.4799	6.87	3.5	−0.7	158	5	156	73
31	8	54.876	35.4809	13.2	4.4	0.1	26	27	16	71
32	9	54.876	35.4808	6.2	4.8	0.7	212	7	42	32
33	10	54.8666	35.4833	4.12	4.6	−0.3	243	67	115	71
34	7	54.8658	35.4825	8.05	3.9	0.3	262	30	207	35
35	7	54.8655	35.4818	6.4	3.6	0.2	73	2	256	35
36	9	54.8652	35.4810	5.56	4.6	0.4	247	52	176	54
37	8	54.8652	35.4799	0.82	2.1	0	136	48	103	64
38	8	54.8658	35.4795	8.79	5.6	−0.5	6	82	288	82
39	10	54.8667	35.4797	0.21	1.2	−0.2	58	11	48	49
40	10	54.8677	35.4804	4.4	9.1	−0.6	105	84	84	88
41	11	54.8693	35.4805	3.88	4.3	−0.1	313	49	163	67
42	10	54.8703	35.4807	11.2	3.2	0.2	97	76	294	86
43	9	54.8713	35.4813	3.61	5.2	−0.8	345	18	332	54

(*Continued*)

Table 1. (*Continued*)

Station	N	Long.	Lat.	Km	P%	T	K1.Trend	K1.Plunge	K3.Strike	K3.Dip
44	9	54.8699	35.4912	13.2	2.5	−0.5	309	40	296	74
45	7	54.8668	35.4898	4.03	1.6	0.4	340	30	175	66
46	13	54.8637	35.4873	3.13	2.4	0.7	192	79	80	80
48	15	54.8648	35.4850	2.99	6.1	0.2	8.9	43.3	201.1	77.3
49	10	54.8665	35.4859	2.83	3.3	0	115.5	28.3	84.1	46
51	10	54.8710	35.4884	3.32	1.5	−0.3	234	1	55.5	43.6
52	11	54.8716	35.4897	8.22	2.1	0.5	73	46	6	48.8
53	12	54.8732	35.4904	10.2	2.8	0.1	1	57	296.5	59.1
54	10	54.8732	35.4910	7.82	1.6	0.2	307	51	304	87.9
55	10	54.8744	35.4871	9.19	2.6	−0.1	131	9	102.4	17.7
56	12	54.8748	35.4848	4.44	1	0.5	16	30	347.6	51
57	10	54.8766	35.4832	8.56	1.6	0.6	170	64	28.2	73.5
58	12	54.8652	35.4865	4.14	2	−0.5	51	55	298.3	57.5
59	14	54.8682	35.4865	0.57	2.2	0.3	54	18	240.2	72.3
60	8	54.8661	35.4834	4.73	7.1	0.7	277	23	121.6	44.3
61	8	54.8695	35.4831	1.97	5.5	0.1	335	61	229.6	61.6
62	10	54.8718	35.4846	3.95	5	0.6	189	51	102.6	51.1
63	11	54.8761	35.4882	7.9	0.9	0.1	126	35	211.2	−31.2
64	7	54.8771	35.4799	6.19	4	0.1	77	86	46.3	87.7
65	12	54.8736	35.4790	4.29	5.1	−0.1	288	31	269.7	62.5
66	8	54.8711	35.4778	7.51	4.8	0	297	11	294.8	78.5
67	11	54.8696	35.4751	10.4	5.2	0.1	90	53	282.4	81.1
68	10	54.8746	35.4752	10.5	3.8	−0.4	163	10	162.7	87.4
69	9	54.8762	35.47805	8.77	5.5	0.5	270	74	263	88.2
70	8	54.8769	35.4855	3.08	1.3	0.3	196	7	100.5	7.2
71	9	54.8779	35.4860	13.2	2.3	−0.1	258	40	91.8	73.6
72	10	54.8799	35.4837	6.4	3	0	15	10	196.5	81.3
73	9	54.8788	35.4794	2.56	0.6	−0.1	17	10	200.1	72.2

Locations (Long./Lat.); n = number of measured specimens; Km = mean magnetic susceptibility [10^{-3}SI]; P% and T = anisotropy and shape parameters; K_1 = magnetic lineation; K_3 = magnetic foliation, plane normal to K_3.

4. Petrography and microstructures

Throughout the intrusion, the fresh diorite of the Chah-Musa body displays no evidence for subsolidus deformation, according to the criteria of Paterson *et al*. (1989) and Vernon (2000). Microscopic examination reveals a porphyritic texture consisting of plagioclase phenocrysts (>30%), needles of hornblende (10%) and biotite books (5%). Microcrystalline plagioclase and hornblende are abundant in the groundmass (Fig. 5a, b), and quartz, apatite, opaques and zircon are accessory minerals.

Euhedral plagioclase laths up to 2 cm in length commonly display a well-developed zonation. Plagioclase exhibits either a clear rim (Fig. 5a, b) or it has a sieved texture. Disequilibrium textures include sieved or dusty plagioclase (Tsuchiyama, 1985) or rounded and embayed crystals (Stimac *et al.* 1990), suggestive of magma mixing or mingling.

Hornblende generally has opaque rims (Fig. 5c, d) or is completely replaced by opaque minerals (Fig. 5g, h). It can be rendered

unstable by melt degassing during decompression (Buckley *et al.* 2006), increase of temperature and/or oxidation of the melt (Rutherford & Devine, 2003).

Books of magmatic biotite are commonly observed in the least altered rocks, especially at the eastern margin of the intrusion. Apatite and some zircon commonly occur as inclusions in opaque minerals, in biotite, and in the groundmass as accessory phases. Magnetite is also a common accessory mineral in the least altered rocks, whereas various associations of pyrite, chalcocite and rutile are typically present in the altered equivalents of these rocks. Anhedral interstitial crystals of sparse quartz are present in the groundmass.

Mineral assemblages indicative of weak propylitic, phyllitic and argillic alterations are common. A zone of weak propylitic alteration occurs in the eastern peripheral parts of the intrusion, where mafic minerals have been transformed into chlorite and calcite.
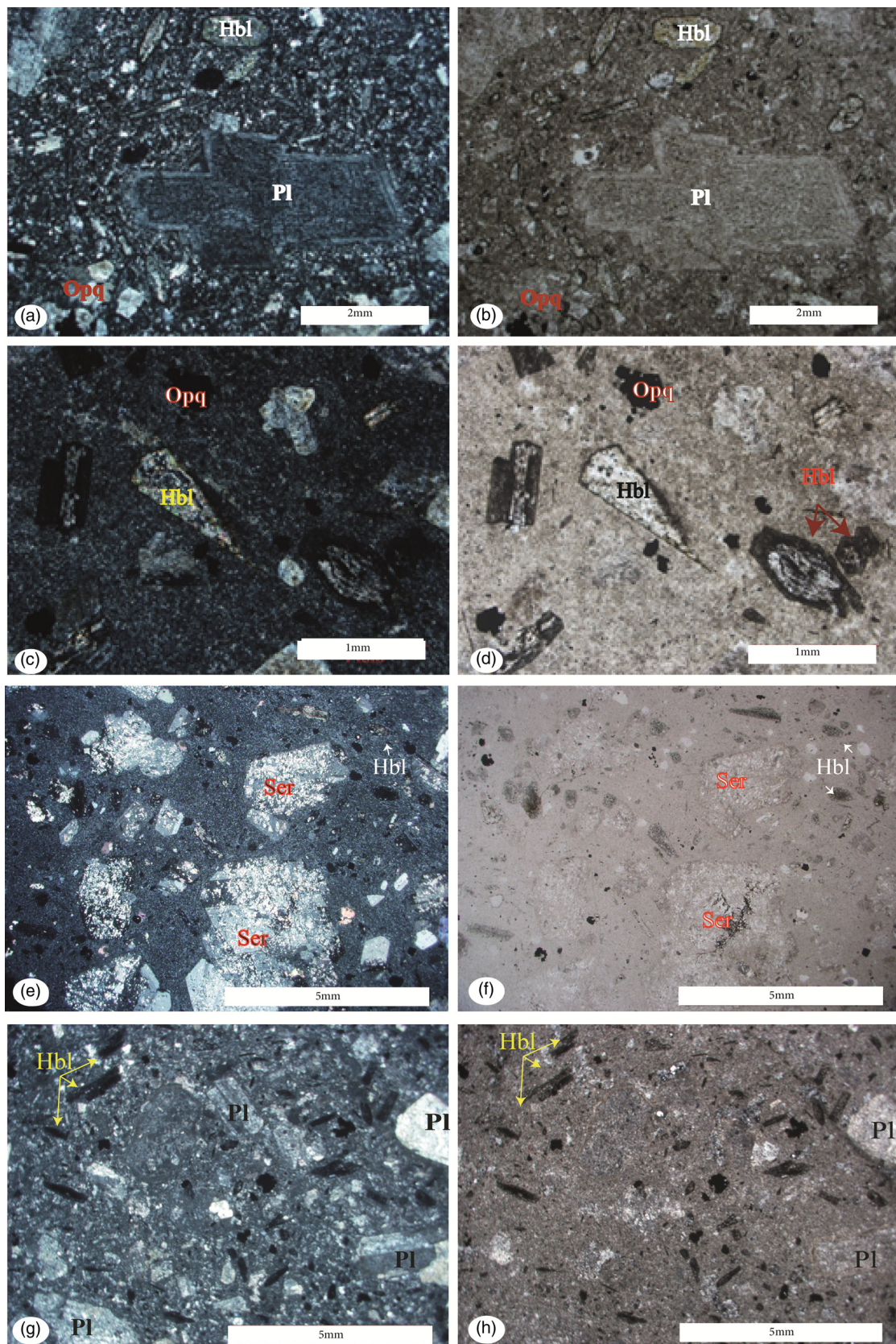
Fig. 5. (Colour online) Representative photomicrographs of texture and mineral assemblages of fresh (a, b) and variously altered rocks from the Chah-Musa intrusion. (a) Sieve texture in plagioclase crystals with a clear rim; (b) (a) at plane polarized light (ppl). (c) Diorite containing plagioclase, hornblende with opacified rims, and opaques (#12); (d) (c) at ppl. (e) Diorite with phyllitic alteration in which plagioclase is altered to sericite (#1); (f) (e) at ppl. (g) Diorite with argillic alteration exhibiting complete replacement of plagioclase by kaolinite (#16); (h) (g) at ppl.
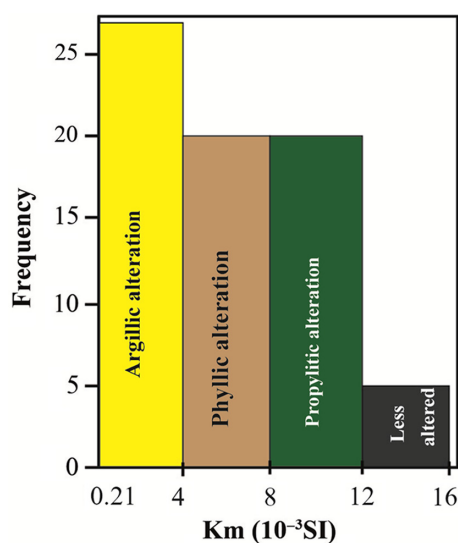
Fig. 6. (Colour online) Magnetic susceptibility histogram (in SI) for different types of altered samples from Chah-Musa intrusion.

In the zone of phyllitic alteration, in the central part of intrusion, plagioclase and hornblende principally are replaced by sericite (Fig. 5e, f) and quartz, accompanied by various amounts of pyrite. Argillitic alteration, which may totally obscure the primary rock texture, is typically characterized by the presence of kaolinite (Fig. 5g, h) and pyrophyllite.

5. AMS analysis

The anisotropy of magnetic susceptibility (AMS) technique provides a rapid quantitative description of the crystal shape fabric in magmatic rocks (e.g. Gleizes *et al.* 1993; Bouchez, 1997; Archanjo & Launeau 2004; De Saint-Blanquat *et al.* 2006; Schöpa *et al.* 2015) and helps to determine the bulk internal structure of a pluton in situations where macroscopic foliation and lineation are weak or absent (Sheibi *et al.* 2012).

5.a. Bulk magnetic susceptibility

Bulk magnetic susceptibility (Km) of rocks, which is the addition of the contributions of the ferromagnetic and the paramagnetic mineral phases (Tarling & Hrouda, 1993), is observed to correlate with field and petrographic observations of alteration. Its magnitude naturally depends on the abundance of the different magnetic minerals, but also on the sizes of magnetite crystals, their chemical compositions, and upon their internal stress and defects (Dunlop & Özdemir, 1997). Susceptibility correlates with alteration, as observed in the field and by petrography (Fig. 6). For fresh and weakly propylitic samples, in which SI ranges from 10 to 15, magnetite acts as the dominant magnetic carrier. Samples that experienced propylitic alteration have a lower magnetic susceptibility. Magnetite being unstable in phyllitic alteration environments (Reed, 1997; Corbett & Leach, 1998; Sillitoe, 2010), this explains the susceptibility decrease in our corresponding samples. The lowest susceptibilities (Km < 0.4 SI) correspond to samples that are both argillitized and located in the vicinity of main faults, where only paramagnetic minerals remain. The magnetic susceptibility contour map (Fig. 7) displays an asymmetrical zonation, with maximum values located along the eastern border and minimum values at the centre and along the western border of the intrusion.

5.b. Opaque mineralogy and magnetic susceptibility

Previous studies have shown that the stability of Fe–Ti oxides is very sensitive to the physical and chemical properties of hydrothermal systems. For example, significant amounts of secondary magnetite may appear during the early stages of potassic alteration (Arancibia & Clark, 1996), whereas circulation of late-stage acidic fluid associated with the phyllitic alteration tends to destroy the magnetite (Beane & Bodnar, 1995). As a consequence the formation, destruction or variation of grain size of the Fe–Ti oxides, as related to hydrothermal fluids, generates a diagnostic magnetic signature in each alteration zone (Sexton *et al.* 1995; Sheibi *et al.* 2016). Idealized models have been proposed to describe such relationships in porphyry-copper deposits (Clark *et al.* 1992; Purucker & Clark, 2011).

To further explore relationships related to alteration, we investigated temperature-dependent magnetic susceptibility in three selected samples (Fig. 8). The less-altered diorite (site #38) displays a dominant ferromagnetic phase (Fig. 8a). An abrupt decrease from 550 °C is consistent with the presence of nearly pure (Ti-free) magnetite (Riveros *et al.* 2014). Figure 8b (sample #16 with phyllitic alteration) exhibits typical low-susceptibility thermomagnetic behaviour where only paramagnetic material is present. From *c*. 440 °C up to *c*. 550 °C, the increase in susceptibility is attributed to the formation of magnetite grains during heating, as attested by the sharp decrease at 580 °C. During cooling, a strong increase of susceptibility starting at 580 °C is observed (Fig. 8b), indicating the continuation of magnetite formation at high temperature. Tudryn & Tucholka (2004) attributed such a thermomagnetic behavior (like sample #16) to altered pyrite. Their experiments illustrate a case in which a paramagnetic mineral, namely pyrite, that cannot be detected by Curie temperature (T_C), can be identified by its transformation into ferrimagnetic phases during heating/cooling experiments. Finally, in the low-susceptibility sample with argillitic alteration (site #39; Fig. 8c) we observe, along with Just & Kontny (2012), that a ferrimagnetic phase is oxidized into hematite, as attested by some susceptibility remaining above 600 °C.

5.c. Magnetic anisotropy (P%) and shape parameter

Anisotropy degree P% is generally used to confirm or extend the deformation zones characterized by microstructural studies. There is generally a positive correlation between P% and the intensity of strain (Borradaile, 1991). However, P% may also correlate with bulk magnetic susceptibility (Km), and thus depend on both mineral composition and strain intensity (Rochette *et al.* 1992). In the Chah-Musa samples, P% ranges from 0.6% to 9.1%, but for 70% of the sites, P% lies between 0.6% and 4.8% (Table 1; Fig. 9). The contoured P% values, using a spline and a first-order polynomial function (Fig. 9), are weakly concentric: the lowest P% is located to the NE and SW margins. Higher P% values appear to the SE and in some isolated sites adjacent to the NW margin of the intrusion.

The T parameter indicates the shape of the magnetic ellipsoid; positive T values (oblate) indicate potential flattening strain, negative T (prolate) indicates potential constrictional strain and T ~ 0 corresponds to plane strain. Roughly concentric isocontours of T exhibit maxima in the outer part of the intrusion, decreasing towards the centre (Fig. 10). Some stations in the eastern half of the intrusion exhibit strongly oblate ellipsoids. Stations characterized by prolate ellipsoids are distributed in the centre of intrusion (near the topographic summit).
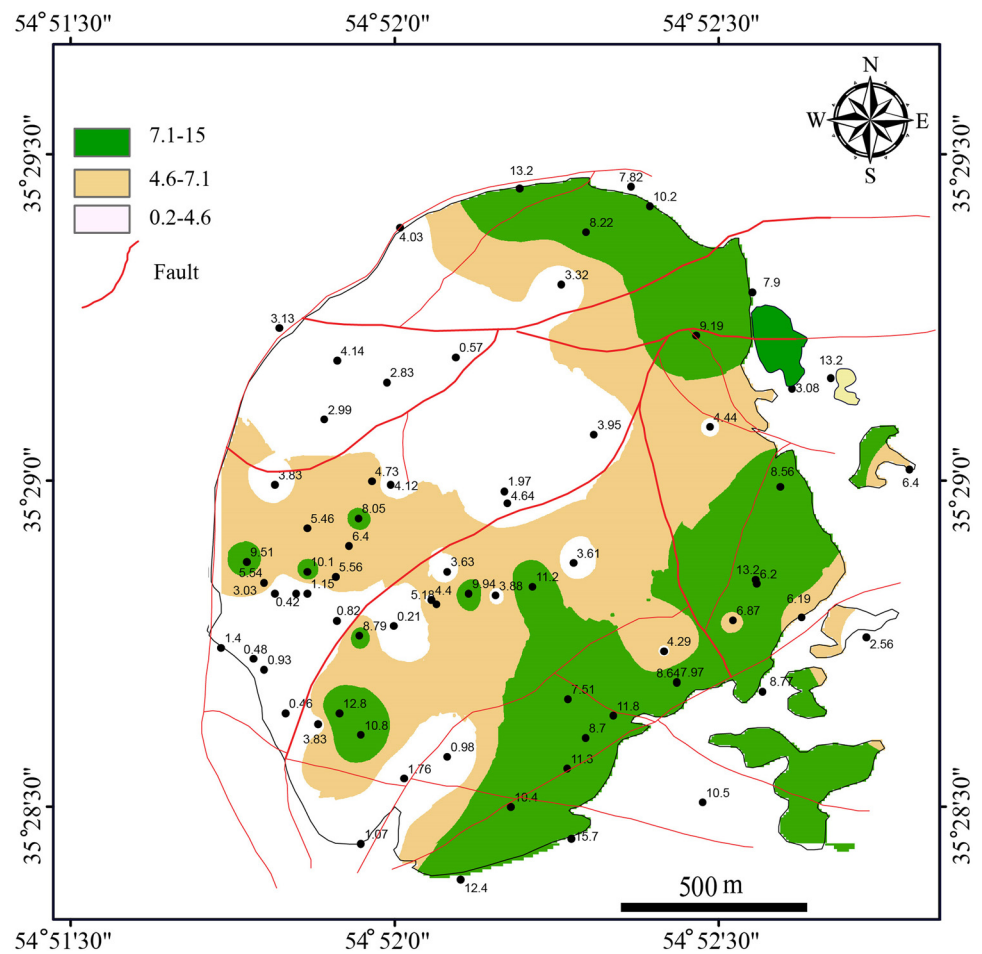
Fig. 7. (Colour online) Magnetic susceptibility contour map (in SI) of the Chah-Musa intrusion.

6. Magnetic fabric patterns

Magnetic fabric of igneous bodies is characterized by the magnetic lineation K_1, and the magnetic foliation perpendicular to K_3 (Hrouda, 1982; Bouchez, 1997, 2000). Magnetic lineations exhibit a relatively concentric distribution pattern in map view (Fig. 11). With the exception of four stations at the NW and SE borders, lineations plunge shallowly in the outer part of the intrusion, and steeply in the central domain, where susceptibility ellipsoids are dominantly prolate (Fig. 11). This suggests that this central part of the intrusion can be considered as a feeder zone. In a density orientation diagram, K_1 is rather scattered with a faint tendency to belong to a girdle and to form a maximum at 43°/53° N (Fig. 12). In map view, dips of foliation are rather concentric and roughly parallel to the contacts of the intrusion. Toward the border of the intrusion (Fig. 13), dips of foliation vary from intermediate to steep (Fig. 13). Due to the more-or-less concentric organization of the foliation planes, an orientation diagram of the foliation poles does not contribute much to the structural information.

7. Discussion

7.a. Hydrothermal alteration and its effects on the magnetic properties

Anisotropy of magnetic susceptibility (AMS) has been applied to the analysis of hydrothermal alterations associated with magmatic intrusions (e.g. Tapia *et al.* 2016). Previous studies have already

pointed out the relationship of hydrothermal alteration to rock magnetic properties (Townley *et al.* 2007; Astudillo *et al.* 2008; Riveros *et al.* 2014). For example, Ade-Hall *et al.* (1971) observed a wide range of opaque mineralogical changes in hydrothermally altered basalt flows. Lapointe *et al.* (1986) suggested the application of magnetic susceptibility as a geophysical index of alteration. Nakamura & Nagahama (2001) reported magnetic and fractal properties of fractured granites from a drill core approaching the Nojima fault, Japan. Xu *et al.* (2003) studied hydrothermal alteration of magnetic fabrics of rocks in the Xiaoban gold-bearing shear belt, Fujian Province, China. Magnetic fabrics (AMS) and magmatic fabrics (shape preferred orientations of plagioclase; SPO) were compared in order to test whether these attributes are interrelated (e.g. Bascou *et al.* 2005) or whether secondary processes such as shock metamorphism and hydrothermal alteration are responsible. Riveros *et al.* (2014) demonstrate a genetic relationship between the hydrothermal alteration processes, Fe–Ti oxide minerals and the magnetic properties of the wall rock in the Escondida porphyry-copper deposit, Chile.

Weathering and alteration may influence the magnetic fabric and, thus, its interpretation. A thorough investigation of the magnetomineralogy is therefore important in the analysis of magnetic fabrics. Hereabove, we have related the magnetic susceptibility to the magneto-mineralogy of the intrusion from a ferromagnetic behaviour in the fresh or less altered samples to a paramagnetic behaviour in the deeply argillitic altered ones. In order to reveal the effect of alteration on the geometry and orientation of
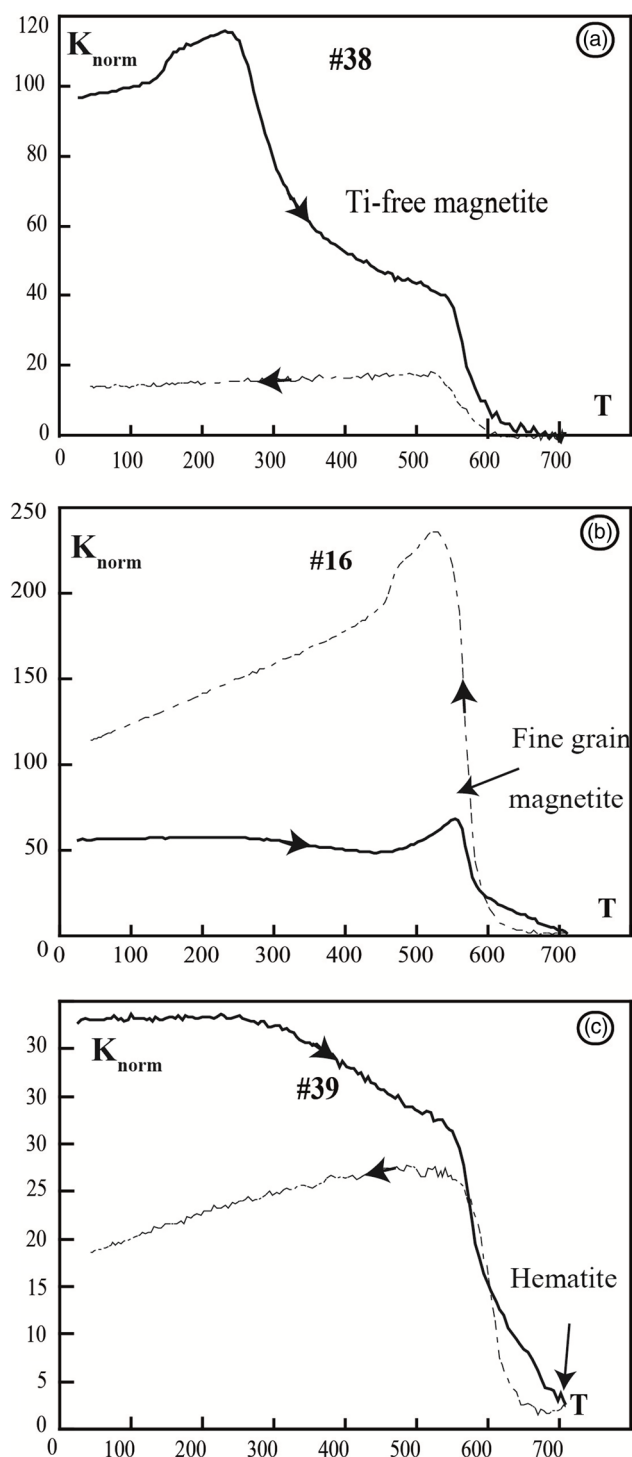
Fig. 8. Susceptibility vs temperature determination of three representative hydrothermally altered rocks from the Chah-Musa intrusion. (Km in SI; T in °C.) K(T) curves with susceptibility normalized to room temperature.

the magnetic fabrics, the anisotropy degree vs the bulk magnetic susceptibility is plotted for the variously altered samples (Fig. 14a). Susceptibility and anisotropy degree are strongly correlated, particularly along fault zones where an argillitic alteration is present. As noted above, the degree of anisotropy correlates both with the intensity of deformation and with magnetic mineral nature and composition. Correlation between P% and strain intensity

in ferromagnetic granites has been a matter of debate. To apply P% as a gauge of strain intensity, we must first demonstrate that P% is independent of Km (Sen *et al.* 2005). Clustering of magnetite crystals can also lead to magnetic interactions, further complicating the interpretation of P% and shape ratios of magnetite crystals (see Archanjo *et al.* 1995). Figures 7 and 9 reveal that areas with high Km (e.g. northern part of the pluton) have low P%. An inverse correlation pertains to diorite samples in the vicinity of the western contacts and supports an alternative interpretation, namely that the magnetic signature is related to strain during emplacement, which increases when approaching the contact. Moreover, for the Chah-Musa pluton no proportional relationship between P% and Km is observable in Figure 14. Microscope petrography of the diorites reveals no significant clustering of magnetite similar to that in the granites studied by Archanjo *et al.* (1995). This agrees with our field observations of an intense deformation of the host rocks and flattened enclaves associated with onion-skin erosion of the porphyritic diorite at the western margins.

Plots of shape fabric parameter vs susceptibility (Fig. 14b) and vs the degree of anisotropy (Fig. 14c) exhibit no correlation between shape and type of alteration, shape of the magnetic anisotropy and bulk susceptibility, nor between the anisotropy degree and the susceptibility. Nevertheless, some stations in the central part of the intrusion with steeply plunging magnetic lineations and prolate ellipsoids can be considered as belonging to the main feeder zone (Fig. 10). Proximity to the roof zone is inferred from the predominantly oblate shape of the magnetic ellipsoid (Fig. 10) and the subhorizontal foliations in the east of the intrusion (Fig. 13). Isolated outcrops having flat-lying cover-rocks onto dioritic rocks are present in the vicinity of these stations. It therefore seems that the magnetic ellipsoids do not substantially change in shape after hydrothermal alteration.

7.b. Regional geological context

Much controversy still persists about how enough space is produced to accommodate intrusive bodies in the upper crust. Magmatism that produced the TCS arc is typical of an activity related to the northward subduction of the Sabzevar–Darouneh branch of the Neo-Tethys ocean. In this arc, structures indicate a special aspect of strike-slip faulted terminations. Khademi (2008) defined two such fault sets in the TCS arc. (i) A mainly compressional set of structures that trend approximately N–S (e.g. east-verging thrust faults and folds involving Palaeozoic and Mesozoic rocks). Dextral and normal shear structures, microfolds, foliations and lineations associated with these structures. (ii) The second set trends NE–SW and includes open gentle folds and younger thrusts verging to the south. These structures involve mainly Cenozoic and younger rocks, but also the older rocks to some degree. The TCS magmatic arc and its bounding faults (Anjilow on the north and Toroud on the south) were involved during the Arabia–Eurasia convergence. A combination of rotation and compression of the Lut block, as part of Central Iran and bounded to the north by the Darouneh fault, led to the transpressional deformation of the studied area (Tadayon *et al.* 2017, 2018).

7.c. Chosen model for the Chah-Musa

The N–S ellipsoidal Chah-Musa intrusion displays rather concentric magnetic lineations and foliations that are consistent with models of ascent and emplacement of elliptical intrusions created by single-blob or nested diapirism, ballooning or laccolith-like
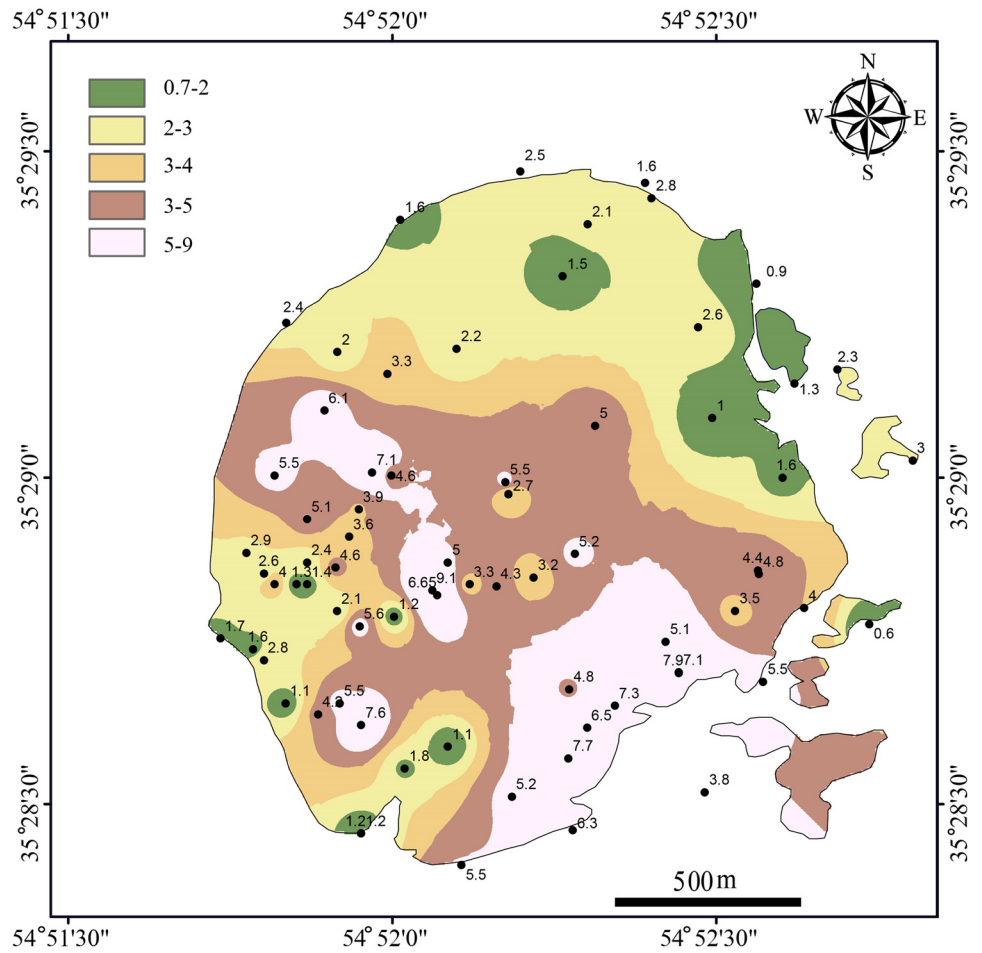
Fig. 9. (Colour online) Anisotropy percentage contour map of the Chah-Musa intrusion.
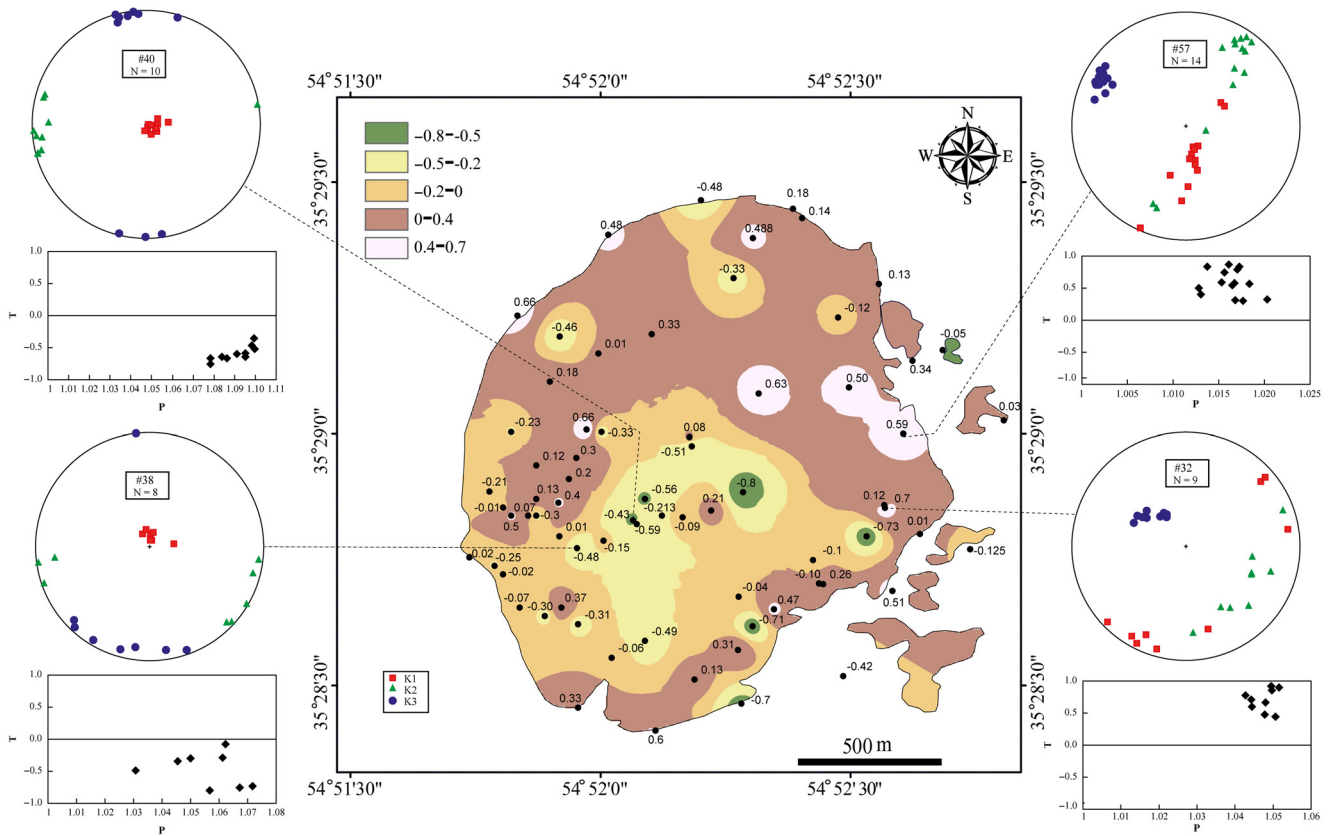

Fig. 10. (Colour online) Shape factor contour map of the Chah-Musa intrusion. Selected stereoplots of magnetic fabrics developed in the feeder zone at the centre and roof zone at the eastern area showing the mean K_1 and K_3 orientations. The anisotropy degree vs ellipsoid shape (P–T) plots of the AMS highlighting variable ellipticity of the magnetic fabric.
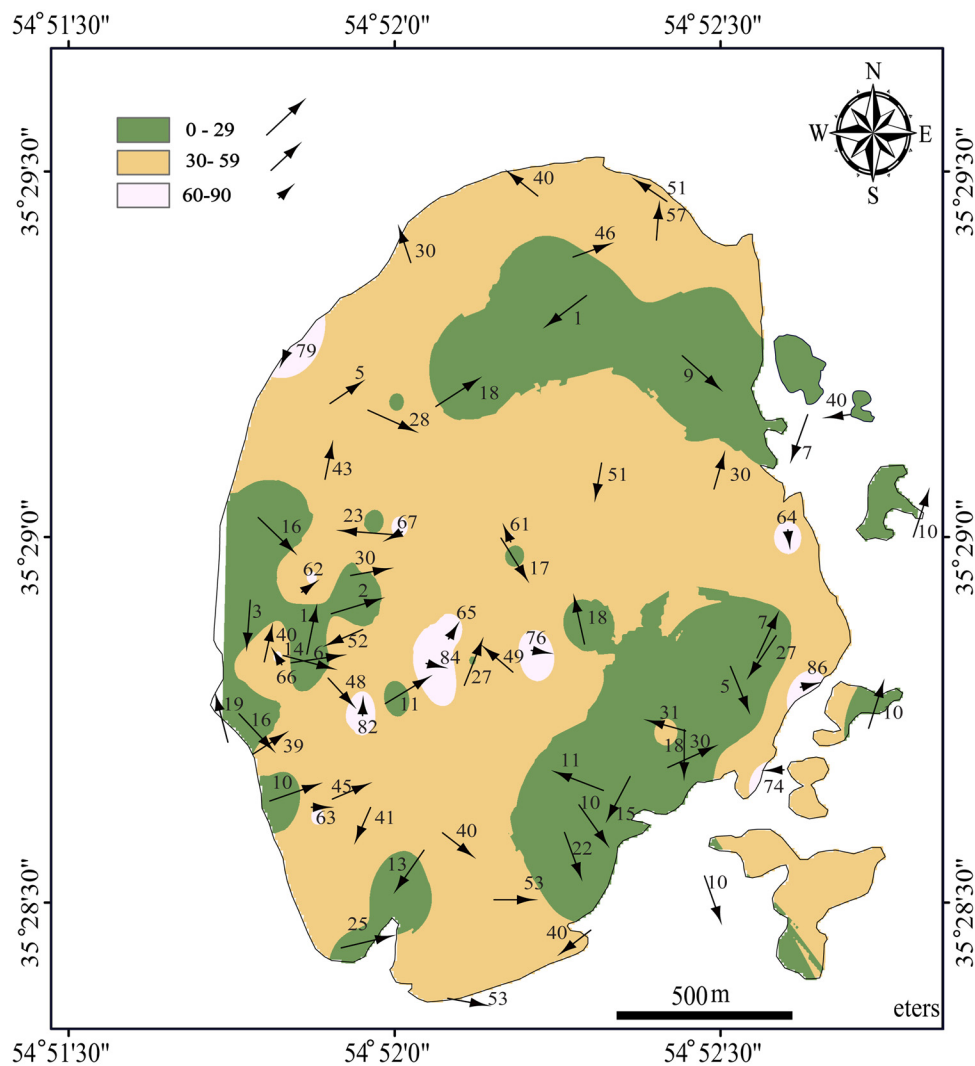
Fig. 11. (Colour online) Magnetic lineation map of the Chah-Musa intrusion. The main magma feeder zone is concentrated in the central area.
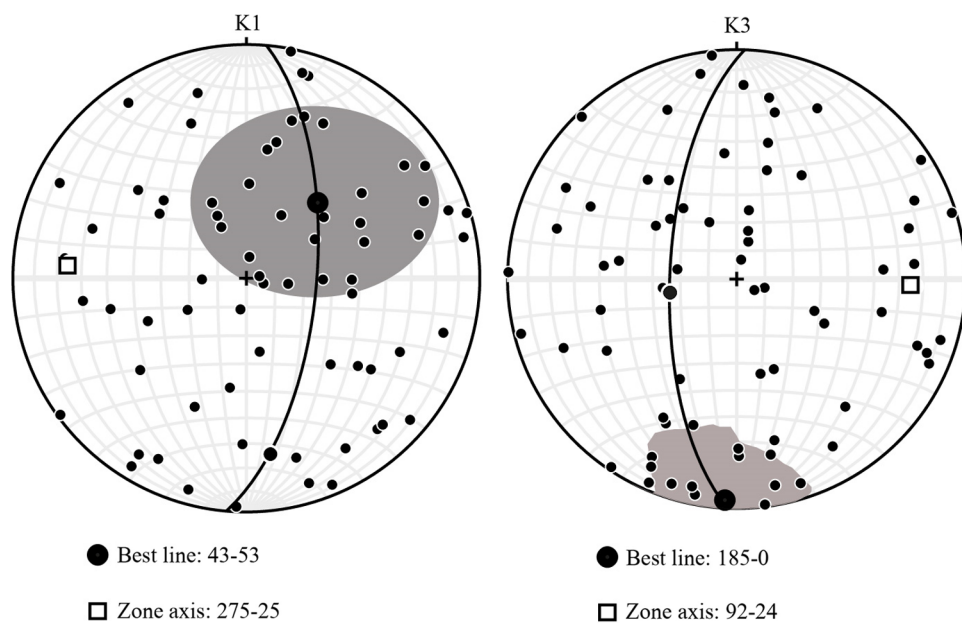

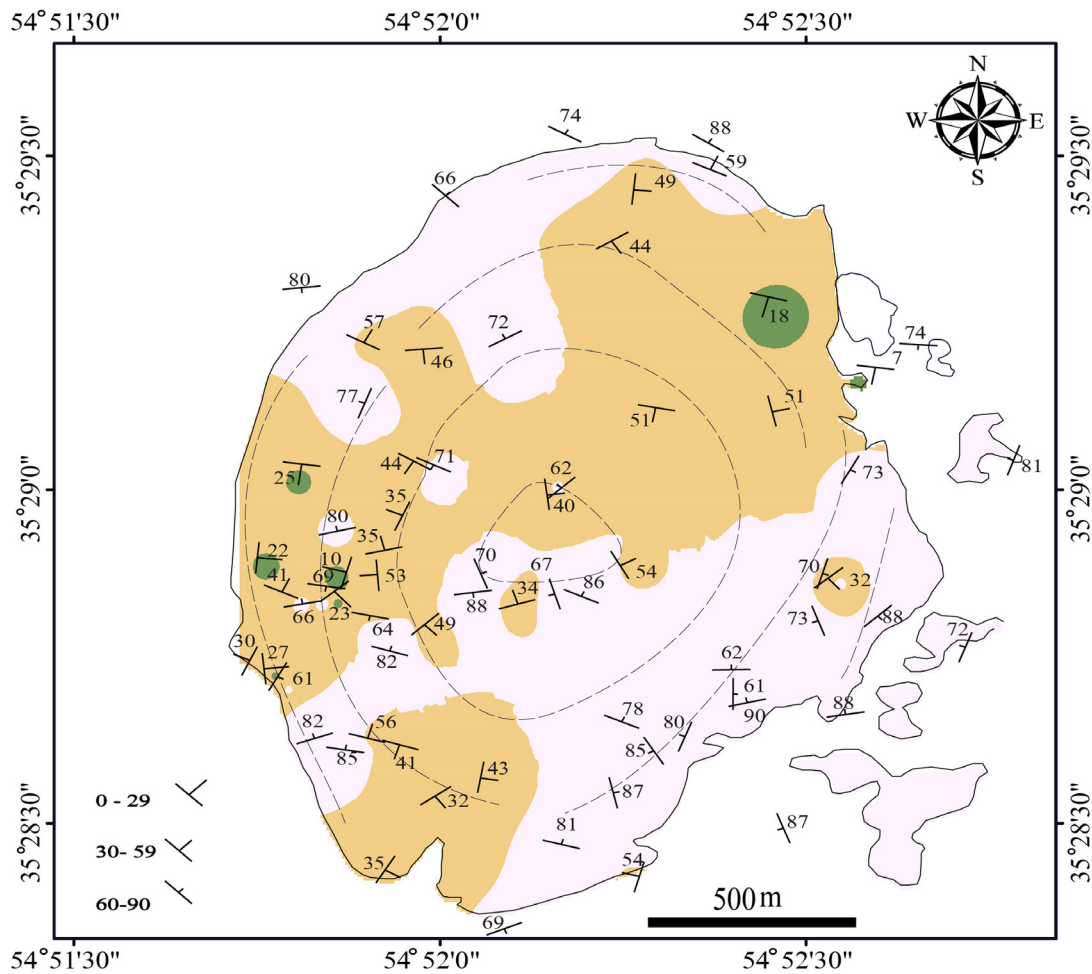**Fig. 12.** Stereoplots representing lineations (K_1) and poles to foliation planes (K_3).

Fig. 13. (Colour online) Magnetic foliation map of the Chah-Musa intrusion. The dashed lines tend to delineate concentric foliation trajectories.

emplacement (see Paterson & Vernon, 1995). Among these possibilities, only doming (Fink *et al.* 1990; Goto & Tsuchiya, 2004), diapirism (Ramsay, 1989) and ballooning or *in situ* inflation of magma (Sylvester *et al.* 1978; Holder, 1981; Molyneux & Hutton, 2000) are able to explain an elliptical intrusion with onion-skin structure revealed by erosion. Otherwise, mutual similarities make it difficult to distinguish between these emplacement models. Assuming that one of the principal stresses is vertical near the free surface, Anderson (1951) demonstrated that the three major classes of faults (reverse, normal and strike-slip) result from the three principal classes of inequality that may exist among the principal stresses. If gravity (i.e. vertically-directed force) is dominant, the result is roof uplift and/or doming (associated with laccolith formation), with superimposed normal faulting in brittle regimes, and boudinage in ductile regimes of the host rock (Anderson, 1951). A horizontally directed positive pressure gradient in magma would lead to reverse or strike-slip faulting in a brittle regime or folding in a ductile regime (Anderson, 1951). However, since normal faulting and reverse or strike-slip fault are not observed among the host rocks of Chah-Musa intrusion, we contend that doming was not a mechanism for the Chah-Musa intrusion.

Diapirism is possible in the ductile lower crust. Some authors (e.g. Marsh, 1982; Vigneresse, 1995) have questioned diapirism as a viable emplacement mechanism. Gravitational ascent is hampered due to insufficient density contrast, heat energy lost to wall

rocks and lacking sufficient buoyancy forces to fracture the brittle crust at the brittle–ductile transition (Vigneresse, 1995). However, the porphyry texture of the rock of Chah-Musa body and the absence of plastic deformation of the host rocks clearly indicate an emplacement at a low level of the upper crust. Petford (1996) argues diapirism cannot be achieved for emplacement in the brittle upper crust. Ballooning is the *in situ* radial inflation of the magma chamber with successively emplaced magmas and bulk shortening of the country rock due to magma injection (Burchardt, 2009). During ballooning, the crystal mush ascends up to the neutral buoyancy level which is the site of final emplacement (JK Becker, unpub. thesis, Georg-August Univ., 2000). Continued injection of magma causes the balloon to expand gradually. The enveloping rocks show signs of pure flattening wherein finite strain ellipsoids parallel the outer margin of the intrusion at all levels (Ramsay, 1989). As a consequence, vertical oblate strain ellipsoids are observed in the equatorial areas of the balloon, and gently outward-dipping, oblate strain ellipsoids are observed in the roof zone. Inside the balloon, a concentric, margin-parallel foliation develops, decreasing in intensity towards the intrusion's centre (Holder, 1981; Clemens *et al.* 1997). Radial lineations develop from the centre of the intrusion and reveal the direction of inflation (Clemens *et al.* 1997).

Microstructural analyses and low magnetic anisotropy observed across the intrusion point to dominant magmatic flow, not to
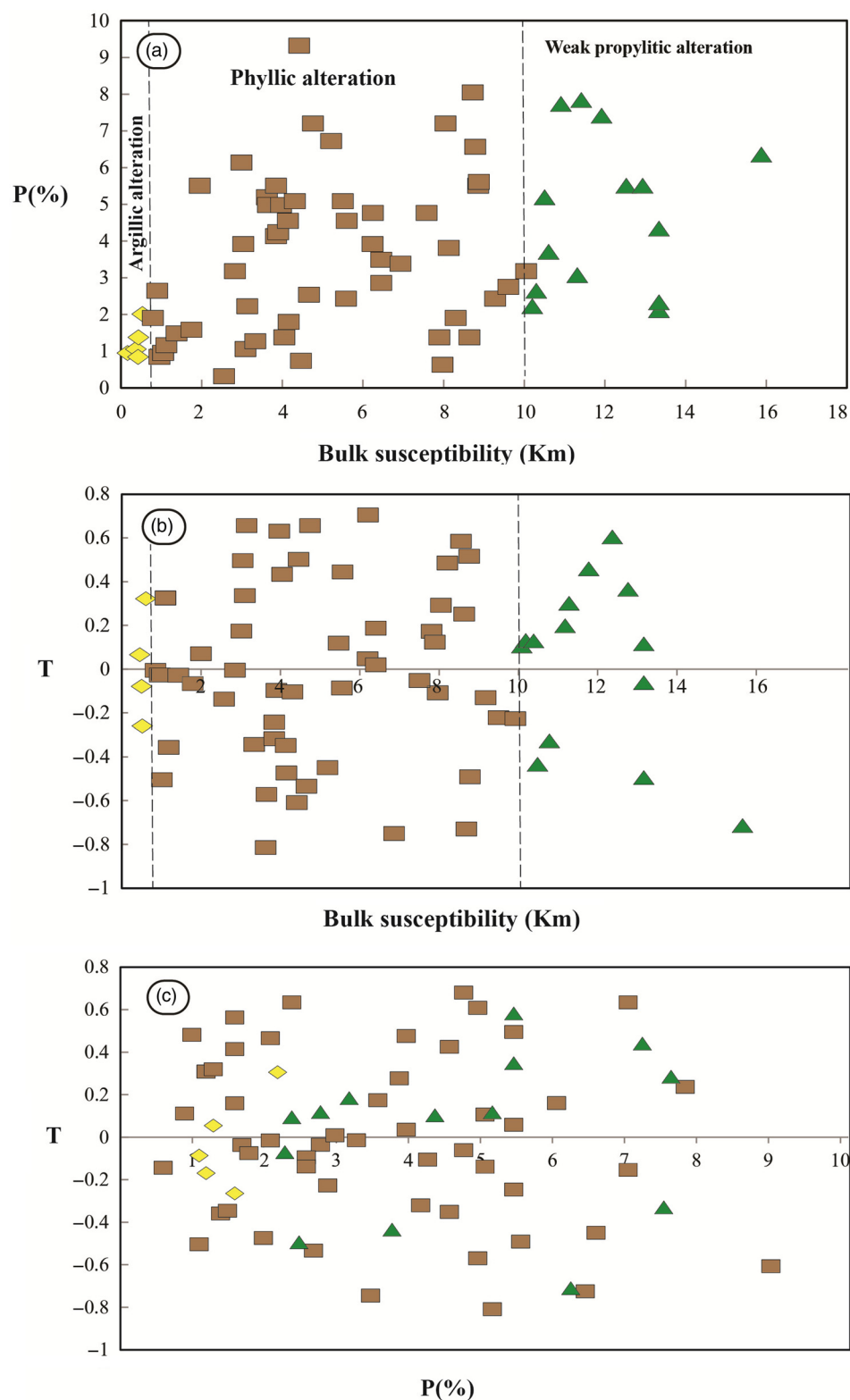
Fig. 14. (Colour online) (a) Susceptibility (Km in SI) vs anisotropy (P%); (b) susceptibility (Km) vs T shape fabric; (c) anisotropy (P%) vs T shape fabric.

solid-state deformation. The liquid/crystal proportion may have been high during emplacement. Pushed aside volcanic rocks enveloping the intrusion at its western margins, and inclined red tuffs and dacitic lava at its northeastern margin, display, however, some solid-state deformation. Moreover, the high values of P% argue for a radial expansion along the WNW–ESE-trending axis of the

intrusion. In addition, the concentric foliations as well as the orientations of long axes of xenoliths parallel to the pluton margins suggest that the strain gradient increased from centre to periphery of the intrusion. Ballooning causes concentric lineations to develop toward the expanding periphery. All of these features point to ballooning as an emplacement mechanism
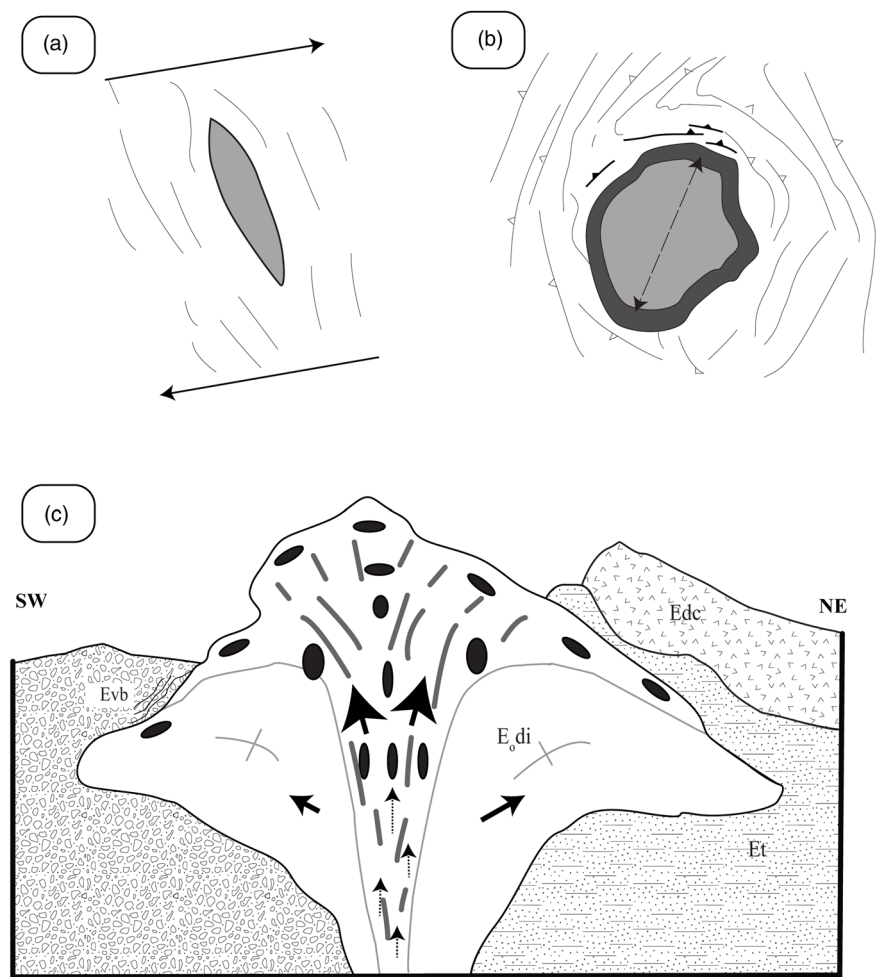
Fig. 15. Emplacement model of the Chah-Musa intrusion through a ballooning mechanism at contact with pyroclastic rocks. (a) Regional scale of dextral shear zone providing tensional spaces required for magma ascent and emplacement. (b) Subsequent expansion of magma and pushing aside of the host rocks through ballooning of magma against pyroclastic rocks at the rheological boundary between andesitic agglomerate, volcanic breccia (E_{ag} & E_{vb}) and red tuffs (E_t); layering in the host rocks is inclined. (c) Geologic cross-sections of the Chah-Musa intrusion and its country rock. Arrows indicate directions of inflation. Ellipses show shape parameter at the feeder zone and roof of the magma chamber.

(Fig. 15). The ballooning at Chah-Musa typifies one of the most common emplacement mechanisms of magmatic bodies at high crustal levels (Antolín-Tomás et al. 2009). Neighbouring plutons such as Kuhe Cheft (Abedini, 2017) and Kuhe Sukhteh (Bakhtavar, 2018) (Figs 1b, 2) share similar attributes.

Structural investigations and models suggest a causal relationship between magma movement and emplacement along strike-slip (Corti et al. 2005), tensional (Hutton, 1988), transpressional (De Saint-Blanquat et al. 1998) and transtensional (Guineberteau et al. 1987) faults. Therefore, the study of the internal fabric of a pluton can be critical to constrain our understanding of the regional tectonics, since magmatism can be associated with both compression and extension (Brown & Solar, 1998; De Saint-Blanquat et al. 1998). Tikoff & Greene (1997) observed that, in transpressional zones, lineations do not necessarily correlate with the direction of magma movement, but rather they reflect changes in the final strain and/or deformation processes affecting an entire region. A model for the emplacement of the Chah-Musa subvolcanic intrusion is proposed in Figure 15. In the eastern parts of the intrusion, the shape parameter suggests that flattening is more intense, a fact that can be interpreted as due to magma pressure against the roof. We postulate that emplacement began as a tension gash that opened parallel to the main stratification of the host rocks and orientated consistent with the early regional E–W dextral shear. As magma was continuously

feeding the gradually expanding chamber, it pushed aside the host rocks at a rheological boundary, i.e. at its contact with the Eocene volcanic rocks.

8. Conclusions

The main conclusions of this study can be summarized as follows:

1. The Chah-Musa intrusion, in NE Iran, is a roughly elliptical and calc-alkaline pluton that was emplaced into an Eocene volcano-sedimentary sequence at upper crustal levels. Rather high susceptibility magnitudes (Km > 0.4 SI) point to a dominant ferromagnetic behaviour. The intrusion experienced weak propylitic (chlorite and calcite), phyllitic (sericite, quartz and pyrite) and argillitic (kaolinite, pyrophyllite and hematite) alteration. Samples with weak propylitic and phyllitic alterations appear in the outer marginal and central part of intrusion, respectively. The argillic alteration is restricted to main faults and fractures. Magnetic susceptibility measurements reveal a progressive transition from ferromagnetic (fresh or less altered rock) to paramagnetic behaviour (deep argillitic alteration). K–T susceptibility is a proxy for the type of rock alteration. Even in the presence of alteration, the magnetic shape factor and to a lesser extent the degree of anisotropy serve as strain markers. Therefore, primary magmatic fabrics of the Chah-Musa pluton seem not to have been affected by alteration.

2. Together, lab measurements of magnetic anisotropy (P%) and field observations of flattened enclaves, intensity of internal foliation, and deflection of host-rock structures indicate a pluton with concentric symmetry, whose floor plunges shallowly except for a steep plunge in the feeder zone. Dioritic magma had ascended through faults planes and ballooned *in situ* in a regional tectonic environment of dextral transpression.

References

Abedini A (2017) *Emplacement mechanism of Kuhe Cheft subvolcanic dome (NW Toroud – South Shahroud) using the anisotropy of magnetic susceptibility method (AMS)*. MSc thesis, Shahrood University of Technology, Shahrood, Iran. Published thesis.

Ade-Hall JM, Palmer HC and Hubbard TP (1971) The magnetic and opaque petrological response of basalts to regional hydrothermal alteration. *Geophysical Journal International* **24**, 137–74.

Anderson EM (1951) *The Dynamics of Faulting and Dike Formation with Applications to Britain*. Edinburgh: Oliver & Boyd.

Antolín-Tomás B, Román-Berdiel T, Casas-Sainz A, Gil-Peña I, Oliva B and Soto R (2009) Structural and magnetic fabric study of the Marimanha granite (Axial Zone of the Pyrenees). *International Journal of Earth Sciences (Geol Rundsch)* **98**, 427–41.

Arancibia ON and Clark AH (1996) Early magnetite-amphibole-plagioclase alteration-mineralization in the Island Copper porphyry copper gold-molybdenum deposit, British Columbia. *Economic Geology* **91**, 402–38.

Archanjo CJ and Launeau P (2004) Magma flow inferred from preferred orientations of plagioclase of the Rio Ceará-Mirim dike swarm (NE Brazil) and its AMS significance. In *Magnetic Fabric: Methods and Applications* (eds F Martín-Hernández, CM Lunemburg, C Aubourg and M Jackson), pp. 285–98. Geological Society of London, Special Publication no. **238**.

Archanjo CJ, Launeau P and Bouchez JL (1995) Magnetic fabric *vs* magnetite and biotite shape fabrics of the magnetite-bearing granite pluton of Gamelerias (Northeast Brazil). *Physics of the Earth and Planetary Interiors* **89**, 63–75.

Astudillo N, Roperch P, Townley B, Arriagada C and Maksaev V (2008) Importance of small-block rotations in damage zones along transcurrent faults. Evidence from the Chuquicamata open pit, Northern Chile. *Tectonophysics* **450**, 1–20.

Bakhtavar E (2018) *Mineral chemistry and emplacement mechanism of Kuhe Sukhteh subvolcanic intrusion (NW Toroud – South Shahrood) using the anisotropy of magnetic susceptibility method (AMS)*. MSc Thesis, Shahrood University of Technology, Shahrood, Iran. Published thesis.

Bascou J, Camps P and Marie Dautria J (2005) Magnetic versus crystallographic fabrics in a basaltic lava flow. *Journal of Volcanology and Geothermal Research* **145**, 119–35.

Beane RE and Bodnar RJ (1995) Hydrothermal fluids and hydrothermal alterations in porphyry copper deposits. In *Porphyry Copper Deposits of the American Cordillera* (eds FW Pierce and JG Bohm), pp. 83–93. Tucson: Arizona Geological Society Digest 20.

Borradaile GJ (1991) Correlation of strain with anisotropy of magnetic susceptibility (AMS). *Pageoph* **135**, 15–29.

Bouchez JL (1997) Granite is never isotropic: an introduction to AMS studies in granitic rocks. In *Granite: From Segregation of Melt to Emplacement Fabrics* (eds JL Bouchez, DHW Hutton and WE Stephens), pp. 95–112. Dordrecht: Kluver.

Bouchez JL (2000) Anisotropie de susceptibilité magnétique et fabrique des granites. *Comptes Rendus de l'Académie des Sciences, Paris. Série IIa. Sciences de la Terre et des Planètes* **330**, 1–14.

Brown M and Solar GS (1998) Granite ascent and emplacement during contractional deformation in convergent orogens. *Journal of Structural Geology* **20**, 1365–93.

Buckley VJE, Sparks RSJ and Wood BJ (2006) Hornblende dehydration reactions during magma ascent at Soufriere Hills volcano, Montserrat. *Contributions to Mineralogy and Petrology* **151**, 121–40.

Burchardt S (2009) *Mechanisms of magma emplacement in the upper crust*. PhD thesis, Georg-August Universität, Göttingen, Germany. Published thesis.

Clark DA, French DH, Lackie MA and Schmidt PW (1992) Magnetic petrology: application of integrated rocks magnetic and petrological techniques to geological interpretation of magnetic surveys. *Exploration Geophysics* **23**, 65–8.

Clemens JD , Petford N and Mawer CK (1997) Ascent mechanisms of granitic magmas: causes and consequences. In *Deformation-Enhanced Fluid Transport in the Earth's Crust and Mantle* (ed. MB Holness), pp. 144–71. London: Chapman & Hall.

Corbett G and Leach T (1998) *Southwest Pacific Rim Gold-Copper Systems: Structure, Alteration, and Mineralization*. Littleton, Colorado: Society of Economic Geologists, Special Publication no. 6.

Corti G, Moratti G and Sani F (2005) Relations between surface faulting and granite intrusions in analogue models of strike-slip deformation. *Journal of Structural Geology* **27**, 1547–62.

De Saint-Blanquat M, Habert G, Horsman E, Morgan SS, Tikoff B, Launeau P and Gleizes G (2006) Mechanisms and duration of non-tectonically assisted magma emplacement in the upper crust: the Black Mesa pluton, Henry Mountains, Utah. *Tectonophysics* **428**, 1–31.

De Saint-Blanquat M, Tikoff B, Teyssier C and Vigneresse JL (1998) Transpressional kinematics and magmatic arcs. In *Continental, Transpressional and Transtensional Tectonics* (eds RE Holdsworth, RA Strachan and JF Dewey), pp. 327–40. Geological Society of London, Special Publication no. 135.

Dunlop D and Özdemir O (1997) *Rock Magnetism: Fundamentals and Frontiers*. Cambridge: Cambridge University Press, 2161–74.

Fard M, Rastad E and Ghaderi M (2006) Epithermal gold and base metal mineralization at Gandy deposit, North of Central Iran and the role of rhyolitic intrusions. *Journal of Sciences, Islamic Republic of Iran* **17**, 327–35.

Fink JH, Malin M and Anderson SW (1990) Intrusive and extrusive growth of the Mount St. Helens lava dome. *Nature* **348**, 435–7.

Fodazi M and Emami MH (2000) Petrology of Mabad Tertiary magmatic rocks (northwest Toroud, Central Iran). In *18th Symposium on Geosciences, Geological Survey of Iran, Tehran*, pp. 224–9. Tehran: Geological Survey of Iran (in Persian).

Fry N (1979) Random point distributions and strain measurement in rocks. *Tectonophysics* **60**, 89–105.

Gleizes G, Nédélec A, Bouchez JL, Autran A and Rochette P (1993) Magnetic susceptibility of the Mont-Louis Andorra ilmenite-type granite (Pyrenees): a new tool for the petrographic characterization and regional mapping of zoned granite plutons. *Journal of Geophysical Research: Solid Earth* **98**, 4317–31.

Goto Y and Tsuchiya N (2004) Morphology and growth style of a Miocene submarine dacite lava dome at Atsumi, northeast Japan. *Journal of Volcanology and Geothermal Research* **134**, 255–75.

Guineberteau B, Bouchez JL and Vigneresse JL (1987) The Mortagne granite pluton (France) emplaced by pull-apart along a shear zone: structural and gravimetric arguments and regional implication. *Geological Society of America Bulletin* **99**, 763–70.

Holder MT (1981) *Mechanics of emplacement of granite plutons*. PhD thesis, University of Leeds, Leeds, UK. Published thesis.

Houshmandzadeh AR, Alavi MN and Haghipour AA (1978) *Evolution of Geological Phenomenon in Toroud Area (Precambrian to Recent)*. Tehran: Geological Survey of Iran, Report H5.

Hrouda F (1982) Magnetic anisotropy of rocks and its application in geology and geophysics. *Geophysical Surveys* **5**, 37–82.

Hutton DH (1988) Granite emplacement mechanisms and tectonic controls: inferences from deformation studies. *Earth and Environmental Science Transactions of the Royal Society of Edinburgh* **79**, 245–55.

Imamjome A, Rastad E, Bouzari F and Rashidnezhad N (2009) An introduction to individual disseminated veinlet and vein mineralization system of Cu (Pb–Zn) in the Chah Musa and Ghole Kaftaran mining district, eastern part

of the Toroud-Chah Shirin magmatic arc. *Geosciences, Scientific Quarterly Journal* **18**, 112–25.

Jelinek V (1978) Statistical processing of magnetic susceptibility measured in groups of specimens. *Studia Geophysica et Geodaetica* **22**, 50–62.

Jones SF, Wielens H, Williamson MC and Zentilli M (2007) Impact of magmatism on petroleum systems in the Sverdrup basin, Canadian Arctic islands, Nunavut: a numerical modelling study. *Journal of Petroleum Geology* **30**, 237–56.

Just J and Kontny K (2012) Thermally induced alterations of minerals during measurements of the temperature dependence of magnetic susceptibility: a case study from the hydrothermally altered Soultz-sous Forêts granite, France. *International Journal of Earth Sciences* **101**, 819–39.

Khademi M (2008) Calculation and interpretation of some morphotectonic indices around the Toruod Fault, south of Damghan. *Geosciences, Scientific Quarterly Journal* **19**, 47–56.

Khajehzadeh MH (2012) *Petrology and geochemistry of north of Moalleman igneous plutons*. MSc thesis, Shahrood University of Technology, Shahrood, Iran. Published thesis, 146 pp. (in Persian).

Khalaj M (2016) Investigation of copper mineralization of Chah Musa, Derakhshanieh and Qolleh Soukhteh area and their relationship with structural linements based on geochemistry, alteration and fluid inclusion in the south of Damghan. MSc thesis, Damghan University, Damghan, Iran. Published thesis, 180 pp. (in Persian).

Lapointe P, Morris WA and Harding KL (1986) Interpretation of magnetic susceptibility: a new approach to geophysical evaluation of the degree of rock alteration. *Canadian Journal of Earth Sciences* **23**, 393–401.

Marsh BD (1982) On the mechanics of igneous diapirism, stoping, and zone melting. *American Journal of Science* **282**, 808–55.

Mehrabi B and Ghasemi MS (2012) Intermediate sulfidation epithermal Pb–Zn–Cu (±Ag–Au) mineralization at Cheshmeh Hafez deposit, Semnan province, Iran. *Journal of the Geological Society of India* **80**, 563–78.

Mehrabi B, Ghasemi SM and Tale FE (2015) Structural control on epithermal mineralization in the Toroud-Chah Shirin belt using point pattern and Fry analyses, north of Iran. *Geotectonics* **49**, 320–31.

Molyneux SJ and Hutton DHW (2000) Evidence for significant granite space creation by the ballooning mechanism: the example of the Ardara pluton, Ireland. *Geological Society of America Bulletin* **112**, 1543–58.

Nakamura N and Nagahama H (2001) Changes in magnetic and fractal properties of fractured granites near the Nojima Fault, Japan. *Island Arc* **10**, 486–94.

Paterson SR and Vernon RH (1995) Bursting the bubble of ballooning plutons: a return to nested diapirs emplaced by multiple processes. *Geological Society of America Bulletin* **107**, 1356–80.

Paterson SR, Vernon RH and Tobisch OT (1989) A review of criteria for the identification of magmatic and tectonic foliations in granitoids. *Journal of Structural Geology* **11**, 349–63.

Petford N (1996) Dikes and diapirs? *Transactions of the Royal Society of Edinburgh: Earth Sciences* **87**, 105–14.

Purucker E and Clark DA (2011) Mapping and interpretation of the lithospheric magnetic field. In *Geomagnetic Observations and Models* (eds M Mandea and M Korte), pp. 311–37. Berlin: Springer.

Ramsay JG (1989) Emplacement kinematics of the granite diapir: the Chindamora batholith, Zimbabwe. *Journal of Structural Geology* **11**, 191–209.

Rashidnejad-Omran N (1992) The Au (Cu) Baghu mineralization: petrological and magmatic evolution relationship. MSc thesis, University of Kharazmi, Kharazmi, Iran. Published thesis.

Reed M (1997) Hydrothermal alteration and its relationship to ore fluid composition. In *Geochemistry of Hydrothermal Ore Deposits* (ed. HL Barnes), pp. 303–365. New York: John Wiley & Sons.

Riveros K, Veloso E, Campos E, Menzies A and Véliz W (2014) Magnetic properties related to hydrothermal alteration processes at the Escondida porphyry copper deposit, northern Chile. *Mineral Deposita* **49**, 693–707.

Rochette P, Jackson M and Aubourg C (1992) Rock magnetism and the interpretation of anisotropy of magnetic susceptibility. *Reviews of Geophysics* **30**, 209–26.

Rutherford MJ and Devine JD (2003) Magmatic conditions and magma ascent as indicated by hornblende phase equilibria and reactions in the 1995–2002 Soufriere Hills magma. *Journal of Petrology* **44**, 1433–54.

Schöpa A, Floess D, De Saint-Blanquat M, Annen C and Launeau P (2015) The relation between magnetite and silicate fabric in granitoids of the Adamello Batholith. *Tectonophysics* **642**, 1–15.

Sen K, Majumder S and Mamtani MA (2005) Degree of magnetic anisotropy as a strain intensity gauge in ferromagnetic granites. *Journal of the Geological Society of London* **162**, 583–6.

Sengör AMC, Cin A, Rowley DB and Nie SY (1993) Space time patterns of magmatism along the Tethys: a preliminary study. *Journal of Geology* **101**, 51–84.

Sexton MA, Morrison GW, Orr TOH, Foley AM and Wormald PJ (1995) The Mt Leyshon magnetic anomaly. *Exploration Geophysics* **26**, 84–91.

Shamanian GH, Hedenquist JW, Hattori KH and Hassanzadeh J (2004) The Gandy and Abolhassani epithermal prospects in the Alborz Magmatic Arc, Semnan Province, Northern Iran. *Economic Geology* **99**, 691–712.

Sheibi M, Bouchez JL, Esmaeily D and Siqueira R (2012) The Shir-Kuh pluton (Central Iran): magnetic fabric evidences for the coalescence of magma batches during emplacement. *Journal of Asian Earth Sciences* **46**, 39–51.

Sheibi M, Mirnejad H and Pooralizadeh Moghaddam M (2016) Magnetic susceptibility anisotropy as a predictive exploration tool of metasomatic iron oxide deposits: example from the Panj-Kuh iron ore body, NE Iran. *Ore Geology Reviews* **72**, 612–28.

Sillitoe RH (2010) Porphyry copper systems. *Economic Geology* **105**, 3–41.

Stimac JA, Pearce TH, Donnelly-Nolan JM and Hearn BC (1990) Origin and implications of undercooled andesitic inclusions in rhyolites, Clear Lake Volcanics, Califomia. *Journal of Geophysical Research* **95**, 17729–46

Svensen H, Planke S and Corfu F (2008) Sill emplacement and contact metamorphism in the Vøring Basin during formation of the North Atlantic Volcanic Province and the implications for the PETM climate change. *International Geological Congress, 6–14 August 2008, Oslo, NorwayI*, Abstract EUR08204.

Sylvester AG, Oertel G, Nelson CA and Christie JM (1978) Papoose Flat pluton: a granitic blister in the Inyo Mountain, California. *Geological Society of America Bulletin* **89**, 1205–19.

Tadayon M, Rossetti F, Zattin M, Calzolari G, Nozaem R, Salvini F, Faccenna C and Khodabakhshi P (2018) The long-term evolution of the Doruneh Fault region (Central Iran): a key to understanding the spatio-temporal tectonic evolution in the hinterland of the Zagros convergence zone. *Geological Journal* **54**, 1–26.

Tadayon M, Rossetti F, Zattin M, Nozaem R, Calzolari G, Madanipour S and Salvini F (2017) The post-Eocene evolution of the Doruneh Fault region (Central Iran): the intraplate response to the re-organisation of the Arabia-Eurasia collision zone. *Tectonics* **36**, 3038–64.

Tajeddin H (1999) *Geology, mineralogy, geochemistry and genesis of Darestan gold occurrences, south of Damghan*. MSc thesis, University of Tarbiat Modares, Tehran, Iran. Published thesis.

Tapia J, Townley B, Córdova L, Poblete F and Arriagada C (2016) Hydrothermal alteration and its effects on the magnetic properties of Los Pelambres, a large multistage porphyry copper deposit. *Journal of Applied Geophysics* **132**, 125–36.

Tarling DH and Hrouda F (1993) *The Magnetic Anisotropy of Rocks*. London: Chapman & Hall, 217 pp.

Tikoff B and Greene D (1997) Stretching lineations in transpressional shear zones. *Journal of Structural Geology* **19**, 29–40.

Townley B, Roperch P, Oliveros V, Tassara A and Arriagada C 2007. Hydrothermal alteration and magnetic properties of rocks in the Carolina de Michilla stratabound copper district, northern Chile. *Mineralium Deposita* **42**, 771–89.

Tsuchiyama A (1985) Dissolution kinetics of plagioclase in the melt of the system diopside-albite-anorthite, and the origin of dusty plagioclase in andesites. *Contributions to Mineralogy and Petrology* **89**, 1–16.

Tudryn A and Tucholka P (2004) Magnetic monitoring of thermal alteration for natural pyrite and greigite. *Acta Geophysica Polonica* **52**, 509–20.

Vernon RH (2000) Review of microstructural evidence of magmatic and solid-state flow. *Electronic Geosciences* **5**(2), 1–23.

Vigneresse JL (1995) Control of granite emplacement by regional deformation. *Tectonophysics* **249**, 173–86.

Xu S, Wu G, Wu J and Chen B (2003) Hydrothermal alteration of magnetic fabrics of rocks in the Xiaoban goldbearing shear belt, Fujian Province, China. *Geofísica Internacional* **42**, 83–94.

Yousefi F, Sadeghian M, Wanhainen C, Ghasemi H and Frei D (2017) Geochemistry, petrogenesis and tectonic setting of middle Eocene hypabyssal rocks of the Toruod–Ahmad Abad magmatic belt: an implication for evolution of the northern branch of Neo-Tethys Ocean in Iran. *Journal of Geochemical Exploration* **178**, 1–15.